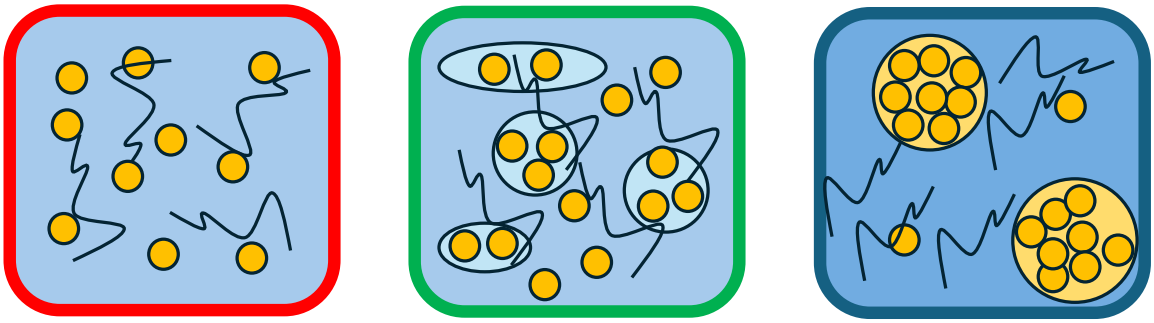

Hydration-induced phase separation in amorphous solid dispersions

A small-angle X-ray scattering study

Master's thesis in Physics, MSc

Simon Dovrén

DEPARTMENT OF PHYSICS

CHALMERS UNIVERSITY OF TECHNOLOGY
Gothenburg, Sweden 2025
www.chalmers.se

Master's thesis 2025

Hydration-induced phase separation in amorphous solid dispersions

A small-angle X-ray scattering study

SIMON DOVRÉN

CHALMERS
UNIVERSITY OF TECHNOLOGY

Department of Physics
Division of Materials Physics
Chalmers University of Technology
Gothenburg, Sweden 2025

Hydration-induced phase separation in amorphous solid dispersions
A small-angle X-ray scattering study
SIMON DOVRÉN

Supervisor: Martina Olsson, Division of Materials Physics
Examiner: Aleksandar Matic, Division of Materials Physics

Master's Thesis 2025
Department of Physics
Division of Materials Physics
Chalmers University of Technology
SE-412 96 Gothenburg
Telephone +46 31 772 1000

Typeset in LaTeX
Printed by Chalmers Reproservice
Gothenburg, Sweden 2025

Hydration-induced phase separation in amorphous solid dispersions
A small-angle X-ray scattering study
SIMON DOVRÉN
Department of Physics
Chalmers University of Technology

Abstract

Amorphous solid dispersions (ASDs) are pharmaceutical formulation in which a drug is molecularly dispersed within a carrier matrix. ASDs are designed to address the challenges of drugs with low solubility in their crystalline state. The carrier matrix, typically a polymer, stabilises the drug in its amorphous phase, which enhance solubility and dissolution rates of the drug.

This thesis examines ASDs composed of the drug indomethacin and the polymer PVPVA as carrier, with the objective to correlate hydration-induced phase separation to drug release behaviour, and test the stability of ASDs in a humid environment. Samples of varying drug concentrations, both pristine and hydrated, were analysed using small-angle X-ray scattering (SAXS), to understand the phase separation processes on the nanoscale. The molecular mobility in the samples was analysed with differential scanning calorimetry (DSC) and the drug release was measured through dissolution tests.

Nanoscale phase separation was found to occur upon exposure to a neutral buffer, for drug loadings >10%, after absorbing >40% buffer. Higher drug load and buffer concentration led to a higher degree of phase separation and the formation and stabilisation of drug-rich domains with distinct interfaces. The phase separation impacted the dissolution properties, as samples with 5% and 10% drug load had faster drug release, in comparison to the samples with 20% and 30% drug load. Phase separation was also found in samples with 30% drug load after being exposed to 98% relative humidity for 10 weeks. The sample did not crystallise, indicating a stable system. These results offer insight into the phase behaviour of ASDs upon dissolution and exposure to humidity, though additional investigation of ASDs in acidic conditions would enhance the understanding of *in vivo* phase separation processes.

Keywords: Amorphous Solid Dispersion (ASD), small-angle X-ray scattering (SAXS), wide-angel X-ray scattering (WAXS), phase separation, homogenuous, heterogeneous, polydispersity.

Acknowledgements

First, I would like to thank my supervisor Martina Olsson and examiner Aleksandar Matic for guiding throughout this project, helping me to stay on track and teaching me about pharmaceutical formulations, X-ray scattering and everything in between. I am vary thankful for the experience of working scientifically, and luring me into five more years at the Materials Physics division.

Additionally, I would like to thank Famke Van Brempt, Arvindh Seshadri Suresh and Anette Larsson at the Division of Applied Chemistry at Chalmers for helping me perform the dissolution test. I would also like to thank Shuichi Haraguchi, also at the Division of Applied Chemistry at Chalmers for preparing the pristine samples. Furthermore, I would like to thank the people at the Materials Physics division for making the last five months a pleasant experience.

Finally, I would like to thank my friends family for supporting me through this Master thesis project and my five years at Chalmers. I would not have enjoyed/endured this time without your company and support.

Simon Dovrén, Gothenburg, June 2025

Contents

1

Introduction

During the last two decades there has been an increase in the fraction of drugs exhibiting poor water solubility and consequently low bio-availability in pharmaceutical development [1]. Amorphous solid dispersions (ASDs) are pharmaceutical formulations in which a drug, in its amorphous state, is dispersed within a carrier matrix. This enhances the solubility and dissolution rates of the drug, increasing bioavailability as more drug is released and absorbed in the stomach. However, the amorphous state is metastable, and the drug can nucleate, and transition to its more stable but less soluble crystalline form [2]. By dispersing the drug in a polymer matrix, the stability can be improved as the polymer decreases molecular mobility of the drug [3]. However, an ASD can also phase separate when hydrated, which may lead to compromised stability and dissolution.

This study specifically examines ASDs composed of the drug indomethacin and poly(1-vinylpyrrolidone-co-vinyl acetate) (PVPVA) as carrier. Indomethacin is a non-steroidal anti-inflammatory drug, mainly used as pain killer. It has low water solubility but exhibits increased dissolution properties in ASDs with hydrophillic carriers [4], [5]. PVPVA is a water-soluble copolymer, commonly used in ASDs [6].

There has previously been dissolution studies conducted on ASDs with indomethacin and PVPVA (IND:PVPVA) [5], [7]. Tres et al. observed that the dissolution rate has a clear drug load and buffer pH dependence. In a neutral dissolution medium (pH 7 buffer), the dissolution rates decreased with increasing drug load, though ASDs up to 90 w% still demonstrated drug release. In an acidic dissolution medium (pH 2 buffer), only ASD with 5 w% drug load exhibited any drug release. Saboo et al. proposed that amorphous-amorphous phase separation occurred in the ASDs with high drug load ($> 10\%$) in an acidic dissolution medium, leading to faster dissolution of the polymer-rich phase, resulting in a drug-rich hydrophobic surface. The poor dissolution behaviour is consequently attributed to formation of a drug-rich layer due to phase separation. The phase separation mechanisms and morphology are however not fully understood and it is also only presented in the case with acidic media, even though there is a drug-load dependence in the neutral dissolution medium. Investigating the phase separation in both cases could reveal the nature of nanoscale processes and how these relate to dissolution behaviour. Additionally, phase separation has been shown to be detrimental to stability, as it can lead to crystallisation of the amorphous drug [8]. Understanding the phase separation will

help future pharmaceutical research to develop more effective and stable ASDs. To achieve this, techniques allowing you to extract information about properties of the nanoscale heterogeneities – such as small-angle X-ray scattering (SAXS) – are of interest. SAXS enables analysis of particle morphology on the nanoscale, which is key in order to understand the phase separation mechanisms.

In this thesis, SAXS is implemented to analyse the phase separation in ASDs after exposure to dissolution media and humidity. The aim of is to link dissolution behaviour of IND:PVPVA ASDs to phase-separation processes during dissolution and during storage in humid environments. With SAXS, differential scanning calorimetry (DSC) and dissolution tests, the phase separation is characterised with respect to drug load and buffer concentration and correlated to dissolution behaviour and phase stability.

2

Background

2.1 Amorphous solid dispersions

Water solubility is key for drug bioavailability, as the drug must be dissolved in the aqueous gastrointestinal fluids [9]. The solubility of a hydrophobic drug can be increased in its amorphous state. In comparison to the crystalline state, the system does not have to overcome the lattice energy barrier in order to dissolve. However, amorphous drugs tend to crystallise over time, as the amorphous state is not thermodynamically favourable. To inhibit crystallisation, the drug can be molecularly dispersed in a carrier matrix. This increases the distances between the drug molecules, making aggregation of drug molecules diffusion limited [9]. If the drug is dispersed within a hydrophilic polymer matrix, the dissolution rate can also be affected. This enhances the wettability of the drug as the surface area is increased, in comparison the pure amorphous drug, resulting in faster dissolution rates.

There are several techniques to process ASDs to ensure that the drug is dispersed within the polymer matrix. One method is hot-melt extrusion [10]. In the process, the polymer and drug is heated while simultaneously mixed by a rotating screw. The viscous mixture eventually reaches the die, where it cools and solidifies as a cylindrical extrudate. This is an efficient processing method, as it is a fast process that can ensure a high degree of mixing.

2.1.1 Amorphous solids

Cooling a liquid slowly can induce a long-range molecular order at the melting temperature, T_{m}, i.e. the liquid transitions into its crystalline state. With a faster cooling rate, the temperature can surpass the melting temperature without crystallising and it becomes a super-cooled liquid, as cooling slows down the molecular kinetics. The crystalline phase is thermodynamically preferred – having lower Gibbs free energy – but due to the longer time scales the molecules cannot rearrange to the equilibrate state [11]. A nucleation could however initiate crystallisation in this state. Cooling even further, the kinetics will be "infinitely" slow in comparison to lab time scales, and the system turns into an amorphous solid. This occurs at the glass transition temperature, T_{g}. This process is illustrated in Fig. 2.1 and is what

one utilises in hot-melt extrusion. A higher T_g indicates lower molecular mobility. The molecules in the amorphous state have short-range order, but lack the long-range order of the crystalline form [12]. The molecular properties are similar to a liquid, while the structural properties are similar to a solid [9]. The lack of long-range order imply larger distances and weaker attractive forces between molecules, enhancing the solubility as there is no lattice energy barrier [3]. When an amorphous drug is dissolved the solution is consequently supersaturated if it surpasses the crystalline solubility. Eventually, the drug would precipitate and the concentration would reach the crystalline solubility. Similarly, pure amorphous drug would eventually crystallise, as the free energy is higher in comparison to the crystalline state. The addition of a polymer can prevent this.

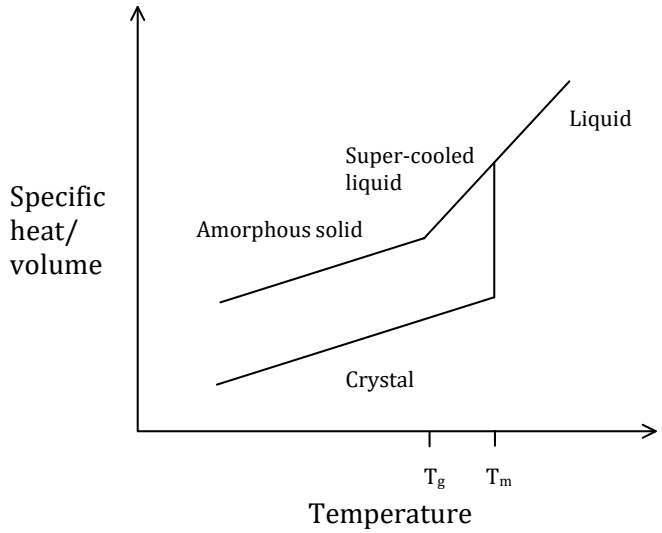

Figure 2.1: Schematic figure of the specific heat and specific volume of a system as a function of temperature. Figure adapted from [9].

2.1.2 Polymer-drug mixing

For optimal ASD behaviour, the drug should be mixed on a molecular level in the polymer matrix [9]. Drug-polymer miscibility is therefore key for the stability and solubility of formulations. In practical cases, the drug-loading has to be high enough in order to have the desired drug uptake to give the intended therapeutic effect [2]. The drug can in those cases be in a supersaturated state in the carrier matrix, and the system is thermodynamically driven towards a favourable state. This implies that phase separation is favoured, and could lead to crystallisation of the drug if initiated. However, it is limited by the kinetics which is slow below T_g.

For a system to be miscible, one must have a negative free energy of mixing:

$$\Delta G_{\text{mix}} = \Delta H_{\text{mix}} - T\Delta S_{\text{mix}} \tag{2.1}$$

where ΔH_{mix} and ΔS_{mix} are the enthalpy and entropy of mixing, and T is the

temperature [9]. The entropy of mixing is defined as:

$$\Delta S_{\text{mix}} = -R(n_{\text{d}} \ln \varphi_{\text{d}} + n_{\text{p}} \ln \varphi_{\text{p}}) \tag{2.2}$$

where R is the gas constant, and $n_{\text{d,p}}$ and $\varphi_{\text{d,p}}$ denote the number of moles and the volume fraction of the drug and polymer, respectively. For the mixed state, $\varphi_{\text{d,p}}$ are always less than one, making $\ln \varphi_{\text{d,p}}$ negative, and consequently the entropy of mixing positive. The contribution to the mixing free energy is therefore negative. The large amount of possible configurations of small drug molecules in between the large polymer molecules results in a large entropic contribution to the free energy. The enthalpy of mixing is defined as:

$$H_{\text{mix}} = H_{\text{dd}} + H_{\text{pp}} - H_{\text{dp}}, \tag{2.3}$$

where dd, pp and dp corresponds to drug, polymer and the mixed systems, respectively. If the drug-polymer interaction is exothermic, the system will release heat, decreasing the enthalpy. For endothermic interactions, the miscibility will be determined by the extent of heat required in comparison to the entropic contribution. The miscibility in ASDs is consequently governed by the drug-polymer interactions.

Dispersing a drug in a polymer matrix also affects the T_{g} of the formulation. In a mixed system, T_{g} will lie between the T_{g}s of the two components. The exact T_{g} will depend on the weight fractions and the intermolecular interactions. A polymer with a higher T_{g}, in comparison to the drug, consequently decreases the mobility of the drug. Water absorption would instead lower the T_{g}, which increases the mobility. Absorbing water in a humid environment or during dissolution could consequently increase the kinetics. If the T_{g} is below the ambient temperature, it is in its supercooled liquid state, in which there is a drastic increase in mobility, possibly increasing the rate of phase separation and crystallisation.

A schematic of a free energy of mixing diagram of amorphous drug and polymer is presented in Fig. 2.2, where the two compounds are thermodynamically treated as liquids, not limited by slow kinetics. The free energy of the system is displayed with respect to the composition of drug and polymer. The diagram illustrates how small fractions of drug added to the polymer would lower the free energy (left-to-right), due to the increase in entropy. The drug would also plasticise, which would increase molecular mobility of the drug [13]. The amount of drug is further increased until there is a local minimum, x_{pd}, in the free energy. The composition at x_{pd} depends on the intermolecular interactions. Up until this point, the system has been stable. Further increasing the drug content pushes the system into a metastable region. At his point, the free energy of the system could be decreased if the system would split into two phases, with composition x_{pd} and x_{dp}. After the inflection point, $\tilde{x}_{\text{pd}}$, the system is unstable, and a spontaneous fluctuations would initiate phase separation. In both cases, the phase separation is thermodynamically driven, as the two phases – drug-rich and drug-poor – would have the compositions of the two local minima, i.e. with the lowest free energy. A similar phenomena is observed when adding a fraction of polymer to the drug (right-to-left).

In the metastable region, phase separation would occur through nucleation and growth. Nucleation would be initiated by fluctuations in concentration, which form small drug-rich droplets [14]. These grow through diffusion form the supersaturated phase. Larger droplets eventually grow at the expense of smaller ones, resulting in coarse drug-rich droplets in a water-rich medium. In the unstable region, the system would phase separate through spinodal decomposition. Unlike nucleation, this process involves continuous fluctuations and does not require overcoming an energy barrier [15]. The system consist of two distinct interconnected phases that coarsen over time, and can be described by characteristic length scale.

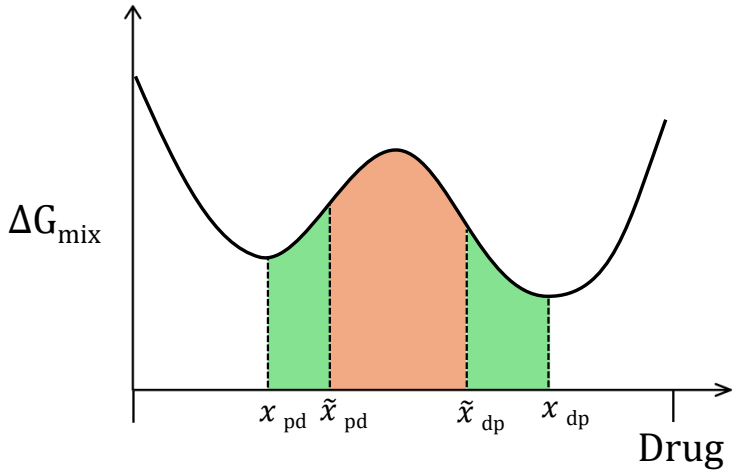

Figure 2.2: Phase behaviour of a two component system of polymer and drug. The x-axis shows the amount of drug in the system. The green marks the metastable region and the orange the unstable region. The regions below x_{pd} and above x_{dp} are the stable regions. Figure adapted from [13].

ASDs are systems with two compounds. Adding dissolution media to this would make it a ternary system. Since dissolution media increases the mobility of the system, this system can be described by Fig. 2.2, albeit with increased complexity. The composition at $x_{\mathrm{d/p,p/d}}$ would not be as clear, as it would also depend on drug-media and polymer-media interactions. One can imagine a drug-rich and a drug-poor phase, but now with the addition of dissolution media, mainly in the drug-poor region due to the hydrophobicity of the drug. The described phase separation have been seen in ASDs after exposure to a humid environment [8]. The absorbed moisture induced amorphous-amorphous phase separation, with different drug-polymer concentrations. This can be detrimental to shelf life of ASDs as it can lead to crystallisation. It has also been observed in ASDs after exposure water [16]. This is relevant for the dissolution properties of ASDs, as it can affect the drug dissolution rates.

2.1.3 Dissolution mechanisms of ASDs

According to Schittny et al., there are three main mechanisms of ASD dissolution: (1) polymer-controlled release, where a polymer gel is formed at the surface during dissolution, through which the drug have to diffuse; (2) congruent release, where the polymer and drug are released simultaneously, leading to fast dissolution and high supersaturation; (3) drug-controlled release, where the polymer on the surface is dissolved, leaving a drug-rich surface layer [17].

Drug load has been seen to have a clear effect on dissolution rate. Saboo et al. examined the dissolution profiles of ASDs consisting of indomethacin and PVPVA, with respect to drug loading in an acidic dissolution media [7]. At low drug loads, up to 10w%, the drug releases congruently with the polymer. At higher drug load, the drug release is inhibited, attributed to amorphous-amorphous phase separation within the ASDs, induced by water absorption. This leads to a faster polymer release on the surface, and eventually the formation a drug-rich surface layer and consequently drug-controlled dissolution.

Tres et al. demonstrated both pH and drug-load dependence on drug release [5]. They looked at similar ASDs of indomethacin and PVPVA in acidic and neutral dissolution media. Only ASDs with 5w% drug load showed drug release. In the neutral media, there was a drug-load dependence as 5w% ASD dissolved quickest. 15% and 30% had similar dissolution profiles, but slower in comparison to 5w%. The dissolution of 5w% in acidic media was attributed to polymer-controlled release, while drug-controlled for the ASDs with higher drug load. In the neutral media, the dissolution was attributed to congruent release.

2.2 Indomethacin and PVPVA

Indomethacin is a non-steroidal anti-inflammatory drug (NSAID), most commonly used as pain relief [18]. It is a class II drug in the biopharmaceutical classification system, as it has poor water solubility and high intestinal permeability [19]. Indomethacin has been shown to have a pH dependent solubility, exhibiting a hundred fold solubility at pH 7.4 compared to pH 1.2 [5], [20]. This is due to the weakly acidic nature of indomethacin, arising from the carboxylic group, as seen in Fig. 2.3a [18], [21], [22]. However, it is still poorly soluble at pH 7.

Poly(vinylpyrrolidone-co-vinyl acetate) (PVPVA), seen in Fig. 2.3b is a synthetic, water-soluble co-polymer, commonly used in ASDs [3]. It forms hydrogen bonds with indomethacin, inhibiting the formation of carboxylic acid cyclic dimers, and consequently contribute to more stable ASDs [22], [24], [25].

As previously mentioned, IND:PVPVA ASDs have exhibited drug-load dependence in dissolution, in both acidic and neutral dissolution media. The drug load effect is not fully understood. In the acidic media, it is attributed to phase separation. Whether the system phase-separates in the neutral media is not known.

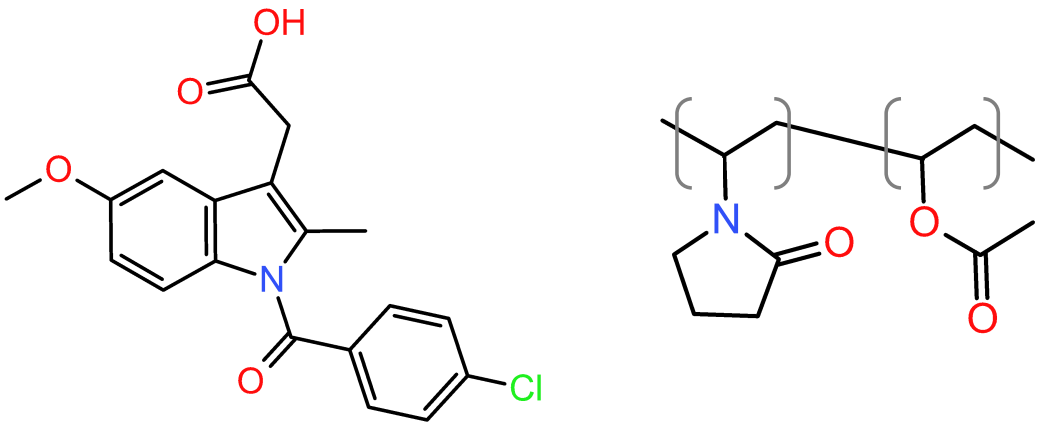

(a) Indomethacin **(b)** PVPVA

Figure 2.3: Chemical structures of indomethacin and PVPVA [18], [23].

2.3 Characterisation techniques

2.3.1 Differential scanning calorimetry

Calorimetric measurements are methods to gain insight to a systems thermodynamic properties [26]. When a system undergoes a phase transitions, the heat flux to or from the sample changes. In differential scanning calorimetry (DSC), the temperature of the system is linearly varied, while the heat flux is measured. This allows for extracting the phase transition temperatures, heat capacity etc. A schematic of a DSC setup can be seen in Fig. 2.4. There are two pans, one containing the sample and one for reference. Both pans are placed on a conductive disc in a furnace, symmetrically around the centre. Thermocouple wires are connected to the disc to measure the temperatures of the two pans. The disc is directly connected to the furnace. It is also connected to an external cooling system, which uses liquid nitrogen from a tank. The furnace heats the disc, and heat flows to the two pans equally, achieving an equilibrium. If the sample undergoes a phase transition, a temperature difference between the two pans will be measured. This difference is proportional to the heat flow. Plotting this heat flow against the temperature allows for determination of the thermodynamic properties.

Fig. 2.5 shows an example of a DSC measurement of a sample undergoing melting and glass transition. It is first heated from room temperature, and melts at $\sim 60\,^{\circ}\mathrm{C}$. This is exhibited by an inverted peak, corresponding to the energy required to melt the sample. When cooled, the samples undergoes a glass transition. This is also seen in the subsequent heating, from where T_{g} is extracted. T_{g} is defined as the midpoint between the intersections of the three tangents, as seen in Fig. 2.5b. It can be noted that the heat of melting is significantly larger in comparison to the glass transition, illustrating the lower heat content of the sample in its crystalline state when compared to its amorphous state, as previously discussed.

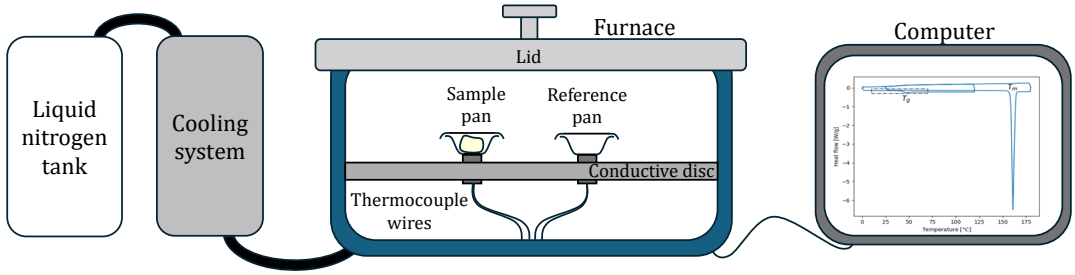

Figure 2.4: Schematic of DSC set-up. Cooling system connected to liquid nitrogen tank and DSC furnace. In the furnace, the two pans are placed on a conducting disc, which is connected to the furnace.

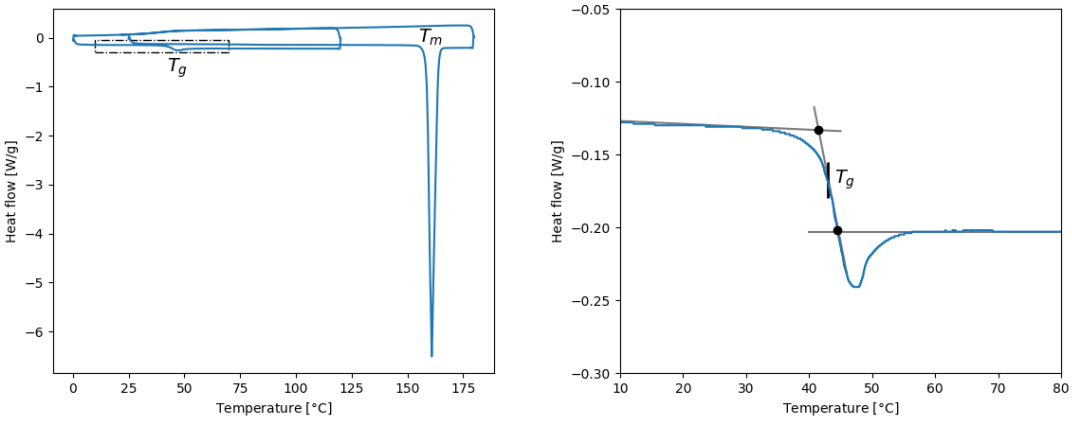

(a) Full DSC measurement starting with glass and melting transition.

(b) Zoomed-in glass transition, with T_g determination.

Figure 2.5: DSC starting at room temperature, where a crystalline sample undergoes a melting transition, indicated by T_m, and then cools without crystallising. At $\sim 40\,°C$, it undergoes a glass transition, indicated by T_g, showing that it is amorphous. The dotted box in (a) show the glass transition, zoomed-in in (b). T_g is defined as the mid-point between the two tangential intersections.

2.3.2 X-ray scattering

X-ray scattering characterises the structure of a system on the Ångström to nanometre length scale [27]. In comparison with microscopy, scattering does not yield a 2D image of the analysed sample. Instead, a scattering pattern is acquired, resulting from photons scattering from all particles in the beam path. The pattern contains information about the average sample structure. The scattering intensity is proportional to the square of the particle volume, and smaller structures will therefore appear less prominent in the pattern, relative to larger structure. Consequently, scattering experiments do not provide a direct image of the sample, but reflect the nanoscale structures of the system.

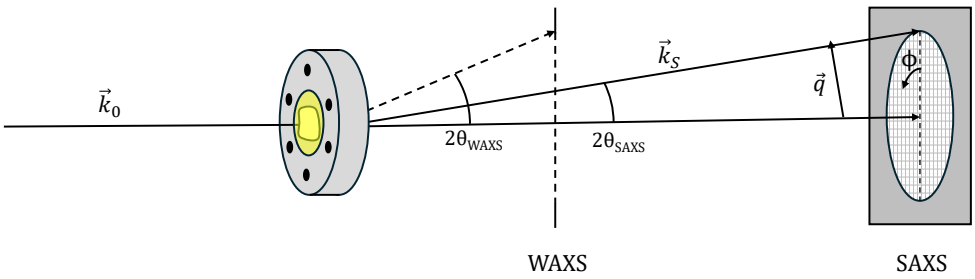

Figure 2.6: Schematic of X-ray scattering measurement with sample in a sandwich cell. Incident photons with $\vec{k}$ scatter off the sample with scattering angle 2θ. Larger distance between detector and sample leads to larger scattering angles, probing smaller lengthscales in the samples.

Fig. 2.6 shows a schematic of an X-ray scattering measurement. The sample is irradiated with an X-ray beam, and the scattered light is detected. The incident photons with wave vector $|\vec{k}_0| = 2\pi/\lambda_0$ interact with the atoms in the sample and are scattered with a wave vector $\vec{k}_s$. The scattering is elastic, i.e. $|\vec{k}_0| = |\vec{k}_s|$ and $\lambda_0 = \lambda_s$. Consequently, interference patterns are recorded on the the detector. The patterns will depend on the particle structures. Specifically, the scattering depends on differences in electron density within the sample, which is referred to as contrast. If there is no contrast between particles and media, no pattern will appear. The pattern can contain both structural and orientational information, yielding the intensity in a 2D-plane, $I(2\Theta, \phi)$, where Θ is the scattering angle and ϕ is the azimuthal angle. If there is no preferred orientation within the sample, the patterns will be isotropic, and the data can be represented 1-dimensionally by integration over ϕ, yielding $I(2\Theta)$. It is commonly redefined to a function of the scattering vector, q, defined as:

$$q = |\vec{k}_s - \vec{k}_0| = \frac{4\pi}{\lambda} \sin(\theta) \tag{2.4}$$

where λ is the wavelength and θ is the scattering angle. The scattering vector q relates to real-space distances d accordingly:

$$q = \frac{2\pi}{d}, \tag{2.5}$$

combining Eq. 2.4 with Bragg's law, showing the inversely proportional relation between q and d [27]. The scattering of all atoms in one particle will result in an interference pattern that is characteristic for the shape and size of that particle, as seen in Fig. 2.7. This contribution to the intensity is called the form factor, $P(q)$. For polydisperse samples, the form factors of all particles add up, creating an average, less distinct, form factor. This is generally the case in practice. For concentrated samples where the interparticle distances are comparable to the particle sizes, there will be additional interference. This interparticle contribution is the structure factor, $S(q)$. The scattering from N_P identical particles with volume V_P

and electron density ρ_{P}, in a medium with electron density ρ_{M} is given by:

$$I(q) = (\rho_{\mathrm{P}} - \rho_{\mathrm{M}})^2 N_{\mathrm{P}} V_{\mathrm{P}}^2 P(q) S(q) + B \tag{2.6}$$

where B is the background scattering.

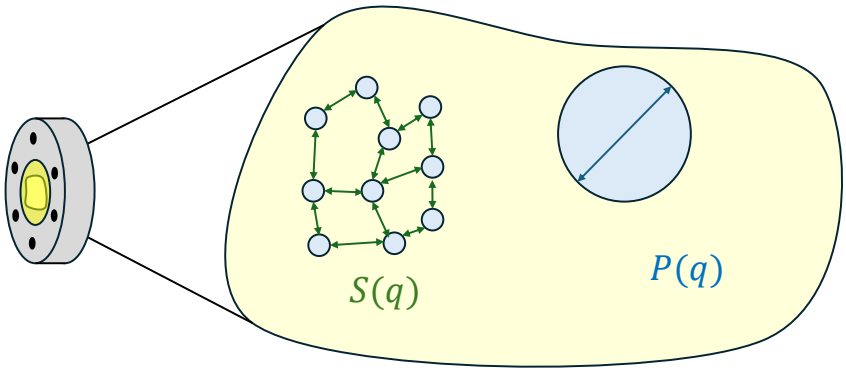

Figure 2.7: Scattering contributions from intra- ($P(q)$) and interparticle ($S(q)$) distances in the sample.

Different q-regions of the detected scattering will contain information on different length scales. Small-angle X-ray scattering (SAXS) measures the intensity at smaller scattering angles, as seen in Fig. 2.6. This corresponds to smaller distances in reciprocal space and, consequently, larger distances in the real space. In this context, larger means a few to a few 100 nanometers. The scattering contains information about the size and shape of the particles and distances between them on this scale. Wide-angle X-ray scattering (WAXS) measures larger scattering angles, corresponding to smaller distances in real space, revealing distances on the atomic scale. WAXS is applicable in determining the solid phase of a material. Performing WAXS on a crystalline material leads to a high degree of interference at the detector due to the long-range order in the material. This corresponds to the interplanar distances, resulting in sharp diffraction peaks. For an amorphous material, the intermolecular distances varies as there is only short-range order, resulting in a distribution of intensities.

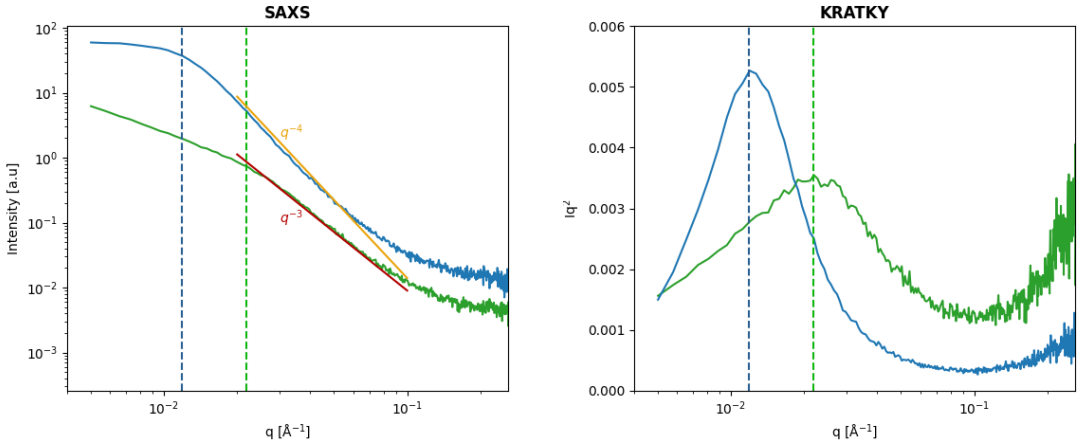

Figure 2.8: Two characteristic SAXS curves in a log-log plot (left) with corresponding Kratky plots (right). In (left) the red and yellow line are q^{-3} and q^{-4} asymptotes, respectively, in the Porod region. The dashed lines corresponds to the two characteristic lengthscales. In (right) the intensity of the green is enhanced by a factor of 10.

2.3.2.1 Model-free SAXS analysis

Modelling SAXS curves is a common approach in SAXS analysis if one has previous knowledge of the morphology of the system to a large extent. If the morphology is less known, this can be difficult and one risks making false claims of the system. In that case, model-free analysis is a more appropriate approach, which is used in this thesis.

In Fig. 2.8, two typical SAXS curves are presented. The Guinier region contains interparticle contributions embedded in the structure factor, $S(q)$ [27]. This typically appears in the low-q region before a form factor $P(q)$ is present, as small q correspond to large real-space distances. This corresponds to the flat part of the blue curve in Fig. 2.8. The region at higher q, the Porod region, instead shows the surface scattering. According to Porod's law, $I(q) \propto q^{-4}$ for larger q corresponds to sharp interfaces according. This is hereafter referred to as a -4 slope. $I(q) \propto q^{-3}$, would indicate rough or non-ideal surfaces. Other slopes could be characteristic of other morphologies. For which q these regions appear in practise depend on the sizes of the probed particles.

When doing model-free analysis, one has to make some assumptions about the system, in order to contextualise any features in the SAXS curves. A constantly decaying curve indicates that there are no electron density fluctuations on the nanoscale in the sample, as it is likely surface scattering from larger particles. Key characteristics, such as shoulders or peaks would indicate a preferred lengthscale in a phase separated system. Distinct features would indicate a characteristic lengthscale, while broad shoulders would indicate polydispersity and an approximate lengthscale. To extract the characteristic or approximate lengthscale, one can use a Kratky plot, Fig. 2.8, where $I \cdot q^2$ is plotted against q. The transition between slopes will here

be illustrated by a peak which can be used to extract a characteristic length scale of the phase separated morphology.

2.3.3 Dissolution tests

In vitro dissolution testing is a standard method to characterise the drug release of solid pharmaceutical formulations [28]. The dissolution media is chosen deepening on which conditions one wants to mimic. A buffer with pH 6.8 should be used to mimic the gastrointestinal fluids [5], [28]. One method of testing is the paddle method, Fig. 2.9a. A rotating paddle stirs the dissolution media and the sample is added to the bath. At set times, aliquots are sampled and analysed in a UV-vis spectrometer to determine the drug concentration.

In a UV-vis spectrometer, visible light is emitted on to a cuvette containing the sample, as seen in Fig. 2.9a. This light is transmitted, scattered or absorbed. As it interacts with a molecule, an electron is initially excited and then de-excites, emitting a photon. The wavelength of the absorbed photon corresponds to the electric energy levels of the drug molecule. If one scans through all wavelengths in a certain interval, an absorption spectrum is acquired, which can be see in Fig. 2.9b. If the molecule of interest is known, Beer Lambert's law can be used to calculate the concentration of the sample [29]:

$$A = \epsilon c l \tag{2.7}$$

where A is the absorbance, ϵ is the molar absorption coefficient, c is the molar concentration and l is the cuvette length. A and ϵ varies with wavelength. To compute the concentration a certain wavelength is chosen, where the absorption is clear and has minimal scattering contribution.

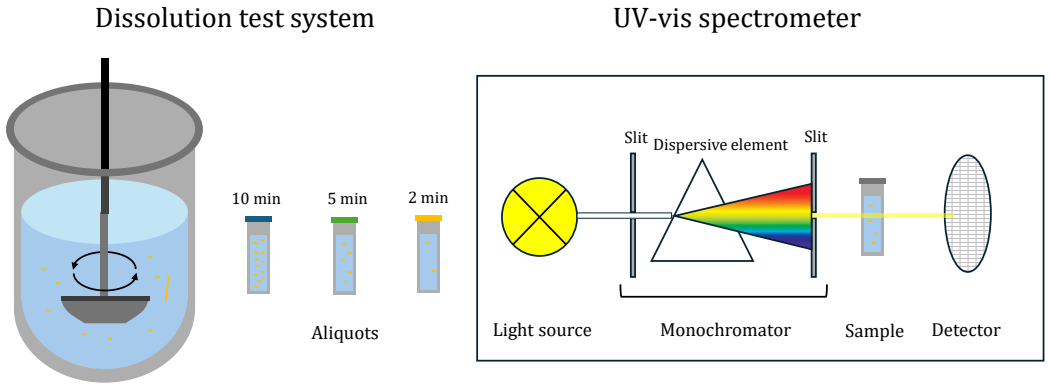

(a) (left) Dissolution test system with rotating paddle and three aliquots sampled at different times. (right) UV-vis spectrometer: Emitted light is filtered through a monochromator. It interacts with the sample and the transmitted light reaches the detector.

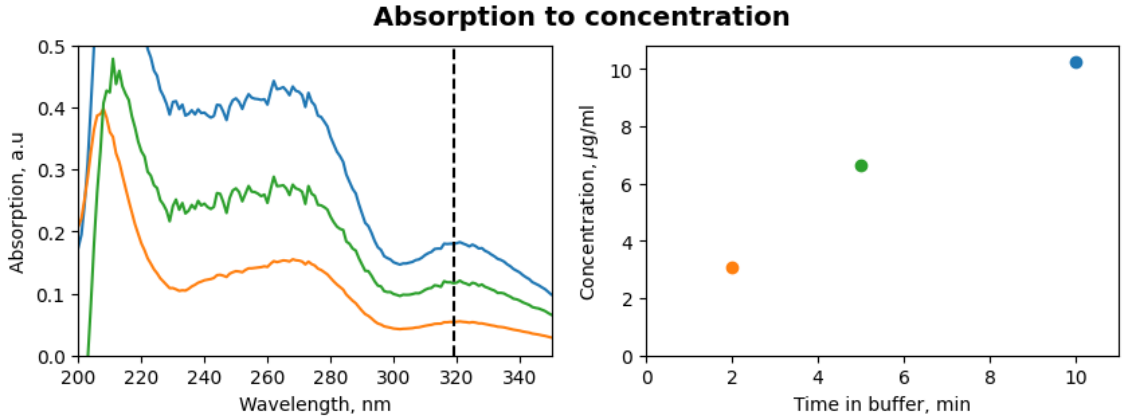

(b) (left) Absorption curves for the three different the three samples aliquots. The dashed line corresponds to the wavelength used for conversion. (right) Corresponding concentrations.

Figure 2.9: The process of determining drug release through dissolution testing: Drug is dissolved in a dissolution bath. The absorption of sampled aliquots is measured with a UV-vis spectrometer, and converted to concentration via Eq. 2.7.

3

Methods

3.1 Material

Amorphous solid dispersions with indomethacin and PVPVA (IND:PVPVA) were prepared with hot-melt extrusion by Shuichi Haraguchi at the Division of Applied Chemistry at Chalmers. Powdered crystalline indomethacin was bought from Sigma-Aldrich. ASDs were prepared with 0, 5, 10, 20 and 30 % drug load. Henceforth, these will be referred to as pure PVPVA, 5:95, 10:90, 20:80 and 30:70. 0.1 M phosphate buffer with pH 6.8 was used as neutral dissolution media, which is used in the majority of the measurements. 0.1 M HCl solution of pH 1 was used as acidic dissolution media.

3.2 Differential scanning calorimetry

DSC measurements were performed for all pristine ASDs with different drug loads. Samples of $\sim$ 5 mg were placed in aluminium hermetic pans. In each measurement, the temperature was ramped from 20 – 180 – 0 – 100+ – 20 °C at a rate of 10 °C min^{-1}. DSC measurements were also made for three samples with added buffer: 10:90, 20:80 and 30:70 with buffer concentrations of 23, 18 and 19%, respectively. These were prepared in the pans and left to equilibrate for 24 hours in sealed containers at room temperature. In each measurement, the temperature was ramped from 25 – 80 – -100 – 80 °C at a rate of 10 °C min^{-1}.

3.3 Small- and wide-angle X-ray scattering

3.3.1 Sample preparation

Hydrated samples were prepared by adding neutral or acidic buffer to a smaller piece of an extruded strand (5 – 20 mg) with a micropipette. The added amount was determined by weight. The buffer concentration is defined as:

$$\text{Buffer concentration } (\%) = 100 \cdot \frac{m_{\text{buffer}}}{m_{\text{pristine}} + m_{\text{buffer}}} \tag{3.1}$$

where m_{pristine} and m_{buffer} are the masses of the pristine sample and the added buffer, respectively. The IND:PVPVA and buffer concentration of all prepared samples can

be found in Tables A.1 and A.2. The samples were equilibrated for 24 – 48 hours.

Six humidity stressed samples were prepared. Four, with drug loads 5:95, 10:90, 20:80 and 30:70, were placed in a desiccator with 75% relative humidity. Two, with drug loads 5:95 and 30:70, were placed in a desiccator with 98% relative humidity. All samples were stored for 10 weeks.

3.3.2 Measurements

The dry samples were taped onto a sample holder. The indomethacin powder and the hydrated and the humidity stressed samples were transferred to sandwich cells. These are sealed, which keeps the them intact in the vacuum chamber of the SAXS instrument. On each side of the cell there is a kapton sheet, allowing the beam to reach the sample. A Mat:Nordic SAXS instrument was used to perform the scattering measurements. The instrument was calibrated with lanthanum hexaboride. The detector distances were 131 and 1081 mm for SAXS and WAXS, respectively. Each sample was measured for 300 s with SAXS and for 100 s with WAXS. Every measurement was transmission corrected. The signal from an empty cell was subtracted for every measurement.

3.4 Dissolution tests

The drug release of all extruded samples with different drug loads were measured in dissolution media of phosphate buffer. All samples were similar in length and mass, varying between 20 – 25 mm and 12.7 – 17.1 mg. The samples were immersed in a dissolution bath with 1000 mL neutral dissolution media at 37 °C. A rotating paddle stirred the bath at 100 rpm.

The drug concentration was measured with a UV-vis spectrometer. A background measurement of phosphate buffer was subtracted from all measurements. The peak at 320 nm was selected to measure the absorption of indomethacin, as it was the most pronounced and had no scattering contribution. Eq. 2.7 with ϵ =6290 $\mathrm{L\,mol^{-1}\,cm^{-1}}$ and cuvette length l =1 cm was used to convert absorption to concentration [18]. A measurement of only PVPVA in neutral dissolution media was made to confirm that it did not contribute to the absorbance, with PVPVA concentration of 39 $\mathrm{mg\,L^{-1}}$, exceeding the maximum PVPVA concentration in the dissolution tests.

4

Results and discussion

4.1 Characterisation of pristine samples

The pristine samples are shown in Fig. 4.1. The yellow tint intensity increases with drug load, as it comes from the indomethacin. The samples are translucent, indicating that they are homogenous, and that there is no microscopic phase separation.

Figure 4.1: Images of the pristine ASDs. From left: PVPVA, 5:95, 10:90, 20:80 and 30:70.

X-ray scattering and DSC measurements of the pristine samples indicate that there is no phase separation on the nanoscale or crystallinity. Fig. 4.2a display the SAXS curves for each ASD together with the neat polymer and drug. No features indicating heterogeneities are seen. The constantly decaying curve indicates that there are no electron density fluctuations. Fig. 4.2b displays the corresponding WAXS curves. Indomethacin shows sharp diffraction peaks, shwoing that the sample is crystalline. All pristine ASDs are amorphous, as the intensities have broad peaks, indicating a distribution of length scales on the Ångström level. It can be noted that the left broad peak decreases with lower polymer content.

Fig. 4.3 show the corresponding DSC measurements. All samples undergo a glass transition. The T_g increase with increased polymer amount, which is expected as the polymer has a higher T_g and antiplasticises the drug, reducing the mobility. The T_gs for the ASDs are above room temperature, as they are solid. The full DSC measurements can be seen in Fig. A.1. All samples exhibit one T_g, supporting a mixed system, agreeing with the translucency of the pristine samples and the SAXS

result. Two T_gs would indicate that there are two phases and that the samples is phase separated.

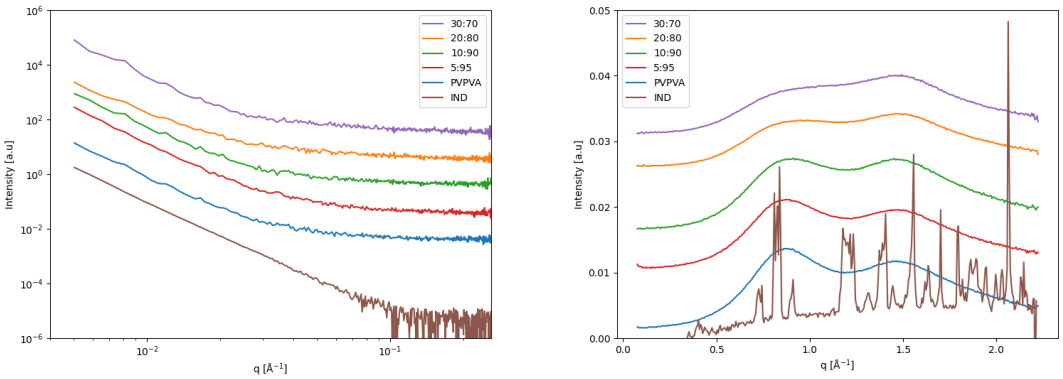

(a) SAXS **(b)** WAXS

Figure 4.2: X-ray scattering measurements of pristine samples. IND is crystalline indomethacin powder, while the other are ASDs. All graphs have been shifted vertically for clarity.

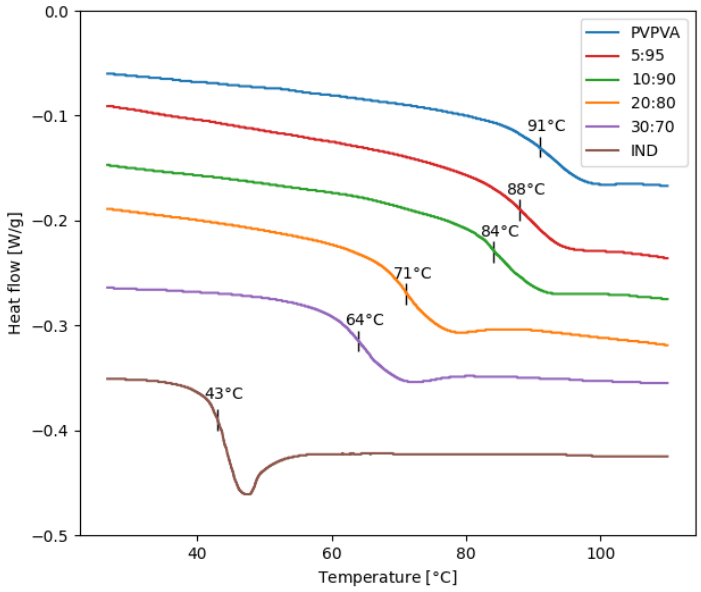

Figure 4.3: DSC measurements of pristine samples. All show only one glass transition, indicating that they are amorphous. The glass transition temperature, T_g, is marked for each the measurement. The full measurements can be seen in the appendix A.1.

4.2 IND:PVPVA in neutral dissolution media

4.2.1 Plasticisation of hydrated ASDs

The pristine samples had T_gs well above room temperature, seen in the DSC measurements in Fig. 4.3. As the ASDs are placed in the dissolution media they are plasticised, and the mobility increases. Fig. 4.4 shows DSC measurements of three hydrated samples with low buffer concentration ($\sim 20\%$). For all samples, the T_g is close to room temperature. This indicates that the mobility in the samples has increased to a large extent. Even higher buffer concentration would lower the T_g below room temperature. This would increase the rate of any ongoing phase-separation or crystallisation processes.

The full DSC measurements can be seen in Fig. A.7. These only contain one T_g, which indicates that no larger scale phase separation or crystallisation has started. It does not rule at nanoscale phase separation as DSC has a finite resolution [30]. SAXS is more sensitive and can therefore also reveal nanoscale heterogeneities.

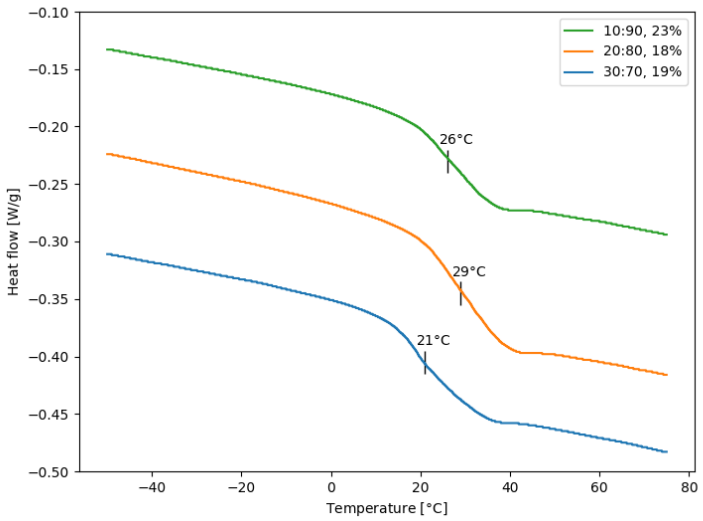

Figure 4.4: DSC of hydrated 10:90, 20:80 and 30:70 samples with 23%, 18% and 19% buffer concentration, respectively.

Fig. 4.5 shows hydrated 5:95 ASDs with varying buffer concentration after 24 hours of equilibration. The sample with 33% buffer concentration is translucent. Samples with higher buffer concentration start showing a faint turbidity, which can be indication of a larger scale phase separation. However, they are still translucent to a large extent and the phase separation is consequently not that widespread. Fig. 4.6 shows hydrated 30:70 ASDs with varying buffer concentration. In contrast to the 5:95 ASDs, all samples are translucent. This indicates that the samples are well-mixed after 24 hours of equilibration, and have not phase separated on a microscale.

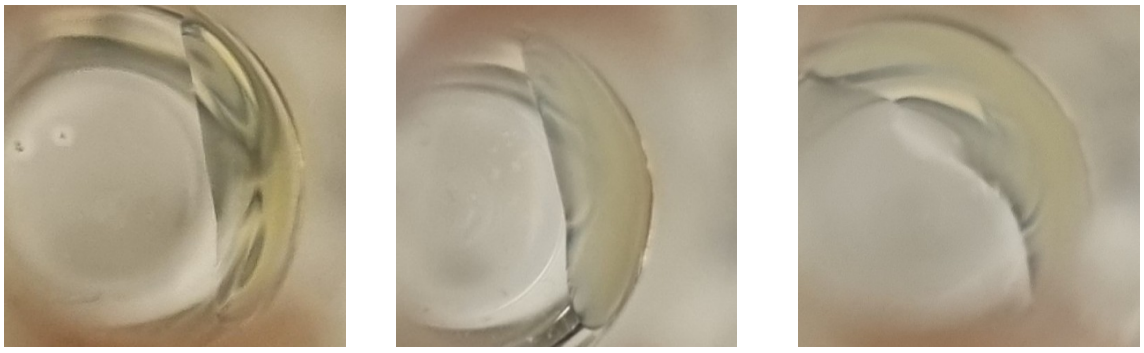

(a) 33% BC. **(b)** 50% BC. **(c)** 65% BC.

Figure 4.5: Images of three 5:95 ASDs with varying neutral buffer concentration (BC) after 24 hours. The 33% sample is translucent, while the 50% and 65% samples are slightly turbid.

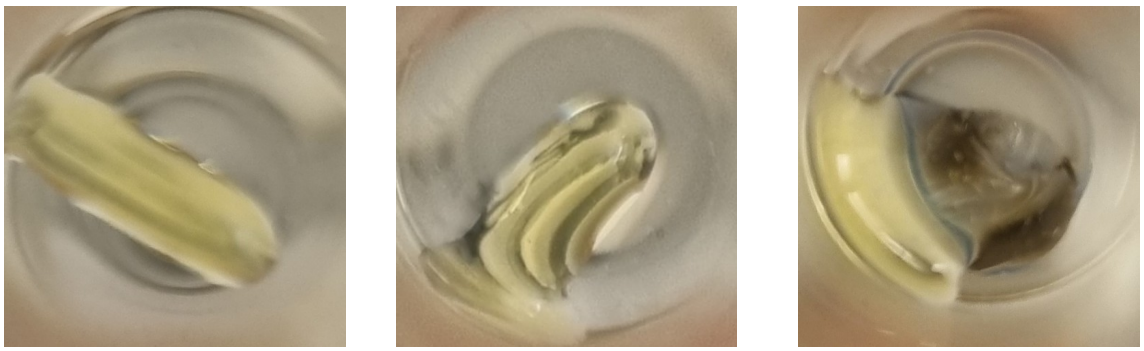

(a) 33% BC. **(b)** 50% BC. **(c)** 70% BC.

Figure 4.6: Images of three 30:70 ASDs with varying neutral buffer concentration (BC) after 24 h. All three samples are translucent.

4.2.2 X-ray scattering revealing phase separation

To detect if nanoscale phase separation occurs during hydration of solid dispersions SAXS and WAXS measurements were performed on samples which have been hydrated with different concentrations of buffer. Fig. 4.7 shows SAXS and WAXS of pure PVPVA ASDs with varying amount of buffer concentration. The SAXS curves in Fig. 4.7a show a low scattering signal or constant decay which shows no evidence of nanoscale heterogeneities as the polymer dissolves. The corresponding WAXS curves in Fig. 4.7b consist of broad peaks, indicative of amorphous samples. The noise can be a result of background subtraction, as the signal is low. The WAXS measurements of the all other samples can be found in Fig. A.2b, A.4, A.5b, A.6b in the appendix. The samples are all amorphous, differing only in intensity, peak position and noise level. All SAXS curves can be found in Fig. A.2a, A.3, A.5a, A.6a. The SAXS figures hereafter contain the characteristic curves for each ASD.

Fig. 4.8 shows four of the SAXS measurements of the 5:95 samples, showing a similar trend of low and constantly decaying signals as the dissolved PVPVA ASDs, indicating a homogenous system.

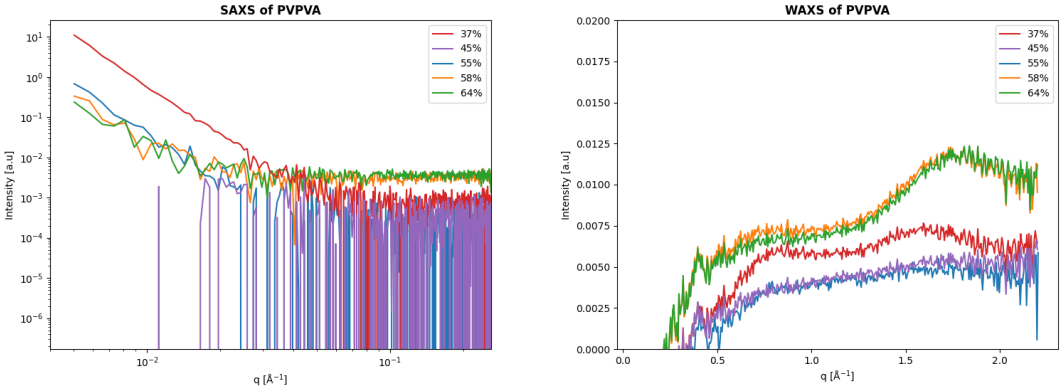

(a) SAXS **(b)** WAXS

Figure 4.7: X-ray scattering measurements of hydrated samples of PVPVA ASDs.

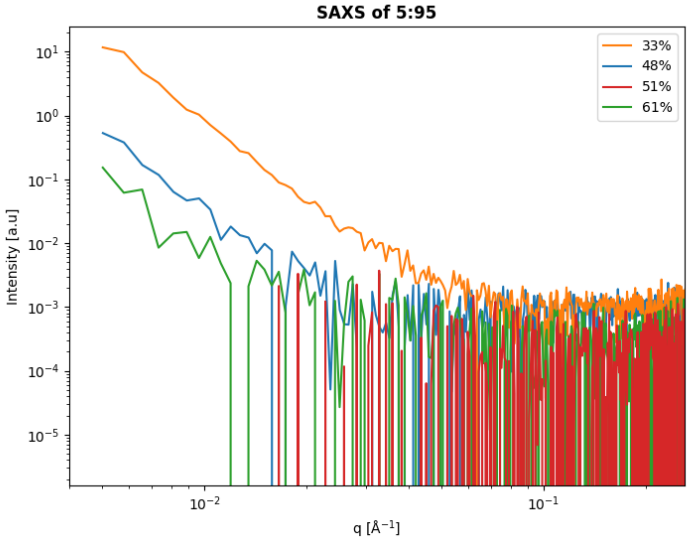

Figure 4.8: Characteristic SAXS measurements of hydrated 5:95 ASDs with varying buffer concentration.

Fig. 4.9 shows characteristic SAXS curves for the 10:90 ASDs. Here, broad shoulders appear at higher buffer concentration, indicating phase separation. The samples with low buffer concentration (<40%) are similar to the corresponding ones for 5:95 and pure PVPVA, showing no indication of phase separation. For higher buffer concentrations (40%-65%), a broad shoulder is visible, indicating nanoscale heterogeneities. Since no similar feature was detected in the PVPVA ASDs, this can be related to phase separation into drug-rich and drug-poor domains. The broad shoulder indicates that there is a large polydispersity in the phase separated structure. However, an average characteristic length scale can be extracted from the midpoint of the shoulder, resulting in an average domain size between 10-30 nm for the different buffer concentrations. Above 65%, a shoulder can be distinguished, though the signal is noisy and disappears for low q. As for the samples with lower drug load,

this is likely due to the sample dissolving.

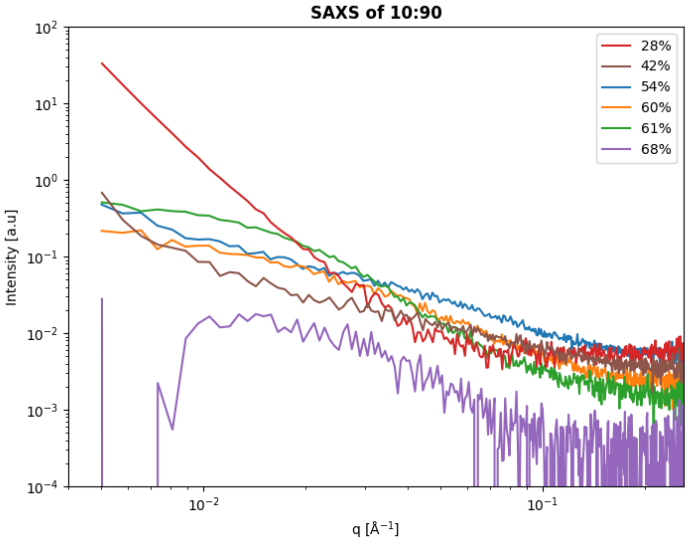

Figure 4.9: Characteristic SAXS measurements of hydrated 10:90 ASDs with varying buffer concentration.

Fig. 4.10 shows characteristic SAXS curves of the 20:80 ASDs. In comparison to the 10:90 samples, the shoulders are generally more prominent. The curves with buffer concentration up to 55% all have shoulders. For the samples with lower buffer concentration (27% and 37%), the shoulders are less pronounced. The shoulders seem to grow in size and shift to smaller q with higher buffer concentration. Similar to the 10:90 ASDs, this indicates polydisperse phase-separated domains with an average size of 10-30 nm.

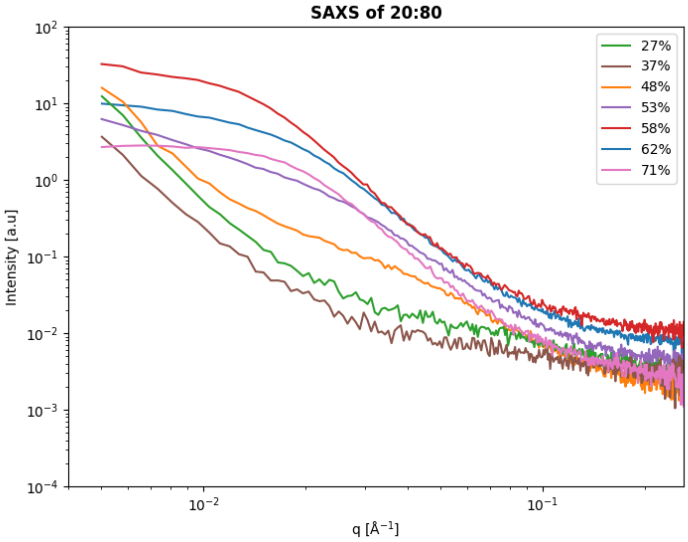

Figure 4.10: Characteristic SAXS measurements of hydrated 20:80 ASDs with varying buffer concentration.

In Fig. 4.11, the average domain sizes are displayed in a scatter plot. This shows that the domain sizes seem to increase with buffer concentration. However, the distribution of length scales indicates that the domain sizes are sensitive to fluctuations in buffer concentration. The curves of samples with higher buffer concentration (>55%) have an even more pronounced shoulder. For these, the slope is ~ -4 for high q. This indicate phase-separated regions with a more well-defined morphology with distinct interfaces. As seen in Fig. 4.11, the characteristic lengthscale, ~ 35 nm, does not vary between measurements. It can be hypothesised that when the buffer concentration is increased above 55%, the drug-rich domains are stable and the added buffer only enters the hydrophillic drug-poor domains. This can be further supported by the curve behaviour at low q. As the buffer concentration increases, the curves flatten in the Guinier region. This can be attributed to a decrease in structure-factor contribution, due to an increase in distance between the drug-rich domains as the drug-poor domains grow.

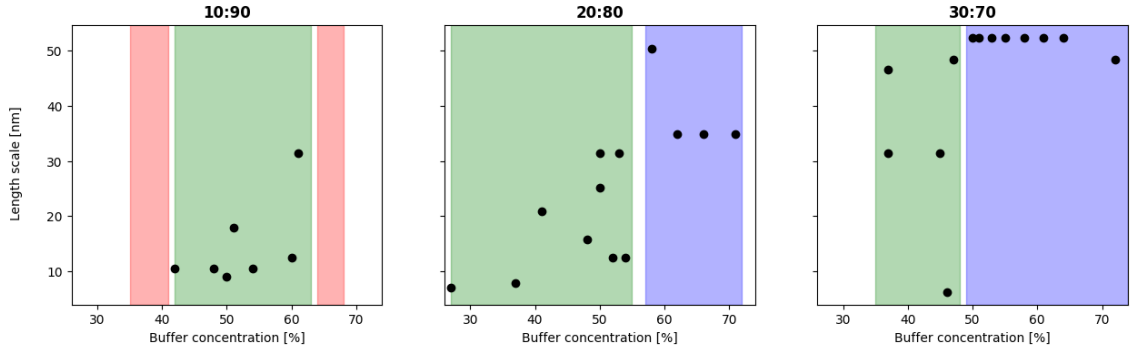

Figure 4.11: Shoulder centre points of measurements indicating approximate or characteristic length scales. The left figure shows 10:90, middle 20:80 and right 30:70. The colours correspond to the regions in Fig. 4.14b.

Fig. 4.12 shows the characteristic SAXS curves of the 30:70 ASDs. For samples with buffer concentration up to 50%, the curves have a shoulder, similar to the 20:80 with lower buffer concentration. This is once more attributed to polydisperse phase separation, but with average domain size of 30-50 nm, as seen in Fig. 4.11. Higher buffer concentrations (>50%) have a more distinct shoulder. For these, the slope is flat in the Guinier region and -4 in the Porod region. As for 20:80, this indicates phase separation into drug-rich and drug-poor domains with distinct interfaces, but with a characteristic lengthscale of 50 nm, as seen in Fig. 4.11.

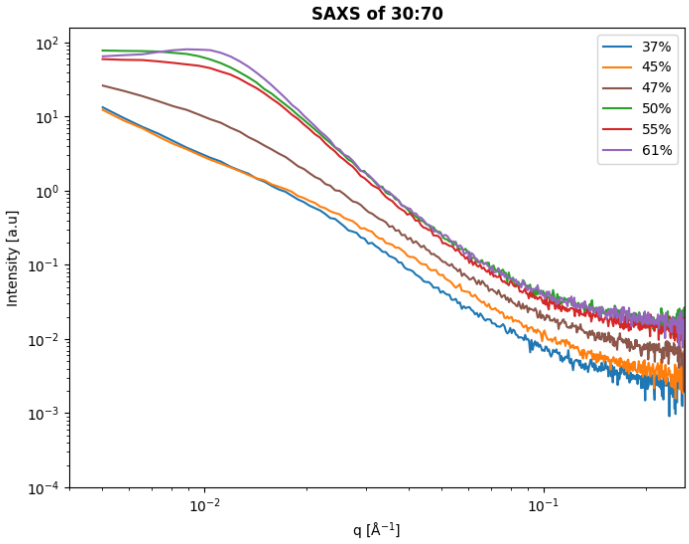

Figure 4.12: Characteristic SAXS measurements of hydrated 30:70 ASDs with varying buffer concentration.

4.2.3 The IND:PVPVA:BUFFER system

To visualise how the phase separated structure with concentration of dissolution media for all ASDs, measurements are displayed in a ternary phase diagram where the structure was divided into five categories based on the scattering signal in Fig. 4.13. The phase diagram has three axes corresponding to PVPVA, indomethacin and buffer concentration. Each dashed line corresponds to the measurements of samples with one IND:PVPVA ratio. A zoomed-in version is presented in Fig. 4.14.

The measurements with no signal or no indication of any frequently occurring length scales are categorised in the red region in Fig. 4.14b. It is believed that the samples in the bottom of this region, where the buffer concentration is low, are not affected to a large extent by the buffer. As the buffer concentration increase, the ASDs dissolve rather than phase separate, if they remain in the red region.

The samples in the green region start exhibiting nanoscale heterogeneities. The SAXS curves indicate a polydisperse structure with an average lengthscale, seen in Fig. 4.11. There is a correlation between length scale and buffer concentration for 10:90 and 20:80, though it is not visible for 30:70. The distribution of lengthscales in this region implies a sensitivity in the domain sizes with respect buffer concentration. The length scales seem to increase within the green region with higher drug load on average. The polydispersity and approximate length scales indicate a morphology that is not well defined, in comparison to the blue region.

The samples in the blue region have a distinct length scale, typically larger than the approximate lengthscale in the green region. The -4 slopes in the Porod region in the SAXS curves indicate that distinct surfaces have been formed. There is therefore a heterogeneity in the system where the length scale is characteristic for

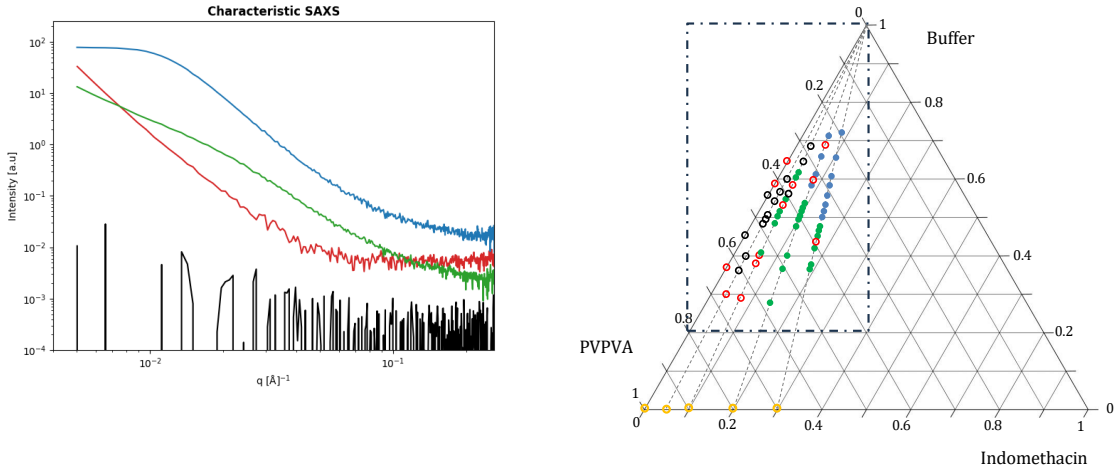

(a) Characteristic SAXS curves.

(b) Ternary phase diagram of IND:PVPVA ASDs and neutral dissolution media.

Figure 4.13: Ternary phase diagram to categorise the SAXS measurements. (a) show the characteristic SAXS curves where the black has no signal and the red has only surface scattering: neither indicates phase separation. These correspond to the black and red circles in (b). The green has a broad shoulder, indicating polydispersity and an approximate length scale and the blue has a distinct shoulder with distinct length scale: both indicate phase separation and correspond to the green and black circles in (b). In (b), yellow corresponds to the pristine samples. A zoomed-in figure of the area in the rectangle is shown in Fig. 4.14a.

the phase separation, and the formed domains are clearly separated at the interface. In comparison to the green region, the length scale does not vary to the same extent between samples. As previously mentioned, it can be hypothesized that the drug-rich domains are more stable after a certain buffer concentration. In that case, the extra buffer content would gather in the drug-poor domains, not affecting the drug-rich domains to a large extent. Similar to the green region, higher drug loads correlate with longer length scale. Continuing the hypothesis, this could mean that more drug would gather in the drug-rich domains, making them larger which increases the lengthscale. The hypothesis is further supported by a the flattening of the curve in the Guinier region for higher buffer concentration, seen for 20:80 in Fig. 4.10. This could indicate a decrease in structure-factor contribution due to more spread-out drug-rich domains.

Additionally, there are outliers in each region, e.g. the red measurements that fall in the green or blue region. The difference in signal in comparison to the surrounding measurements could be due to inhomogeneities along the strand in the ASD extrudates. Regions with different morphology could also have formed within the sample, and the X-ray beam only interacts with one.

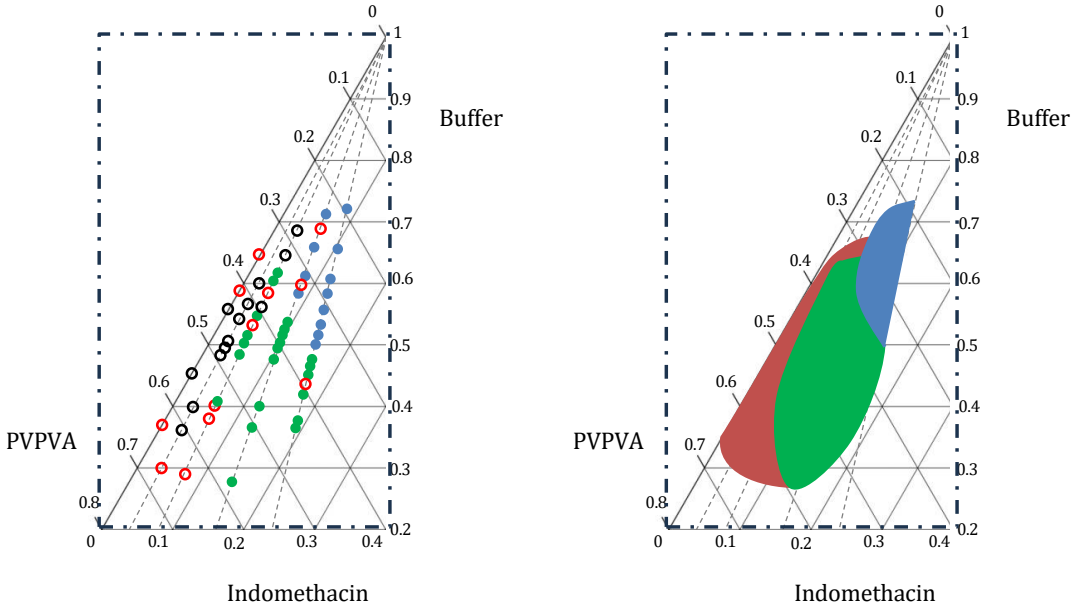

(a) Zoomed-in version of Fig. 4.13b. **(b)** Generalised diagram.

Figure 4.14: Zoomed-in versions of the ternary phase diagram in Fig. 4.13b. The measurements in (a) are generalised as three regions in (b), where they correspond to three different characteristic SAXS measurements.

4.2.4 Correlating phase separation and dissolution

The release curves of the ASDs with different drug load are presented in Fig. 4.15. The curves are normalised with respect to the maximum amount dissolved drug for each sample. All ASDs were fully dissolved within 10 minutes. This indicates that the phase separation described above has no substantial effect on the drug release, and that phase separation is not inherently detrimental for dissolution of ASDs. After 4 minutes of dissolution the 5:95 and 10:90 samples have similar behaviour. The same can be said for the 20:80 and 30:70 samples. This can be a consequence of the distinct phase separation with stable drug-rich domains and clear interfaces, seen for higher drug concentrations in the 20:80 and 30:70 samples.

A similar behaviour was seen by Tres et al. as they performed non-sink dissolution tests of IND:PVPVA ASDs [5]. In a neutral dissolution media, they saw similar dissolution behaviour for 15:85 and 30:70 samples, while the 5:95 sample had faster release. One could hypothesize that the distinct phase separation seen in 20:80 and 30:70 hinders congruent release of drug and polymer to some extent, leading to the slower drug-release rates. This can be compared to the study by Saboo et al, who performed dissolution tests of IND:PVPVA ASDs in an acidic dissolution media [7]. For 5:95 and 10:90 ASDs they saw congruent release, while they saw incongruent drug release for 15:85 and 25:75 ASDs, attributed to the formation of drug-rich and drug-poor domains. It should be made clear that the dissolution behaviour is very different in acidic and neutral dissolution media.

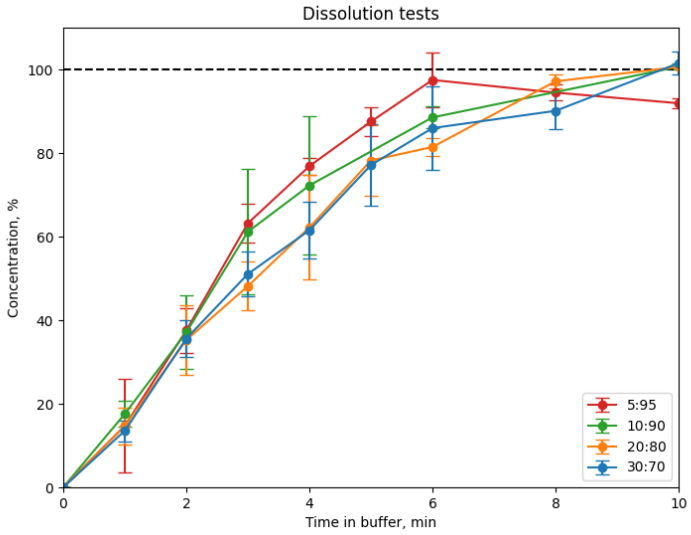

Figure 4.15: Release curves of 5:95, 10:90, 20:80 and 30:70. For each ASD, two dissolution tests were made. The maximum concentration is normalized with respect to the weight of the sample.

It should also be noted that the phase separation in this study is found in samples that have equilibrated for 24 hours, in comparison to the 10 minutes of the dissolution tests. However, the dissolution media drastically increases the mobility, which would increase the rate of the phase separation that is now known.

4.2.5 ASDs in acidic media

To compare the phase separation mechanisms during dissolution, ASDs were hydrated with varying concentrations of acidic dissolution media. Fig. 4.16 shows hydrated 5:95 samples, equilibrated for 24 hours. The sample with low buffer concentration is translucent. However, increasing buffer concentration increase the turbidity of the samples. In comparison to the 5:95 samples with neutral dissolution media, these are more turbid, indicating a more pronounced microscale phase separation.

Fig. 4.17 shows images of 30:70 ASDs hydrated with acidic buffer and equilibrated for 24 hours. They became opaque with 30% buffer concentration, indicating microscale phase separation. This can be compared to the 30:70 samples hydrated with neutral dissolution media, which remained translucent as the buffer concentration increase. Here, the samples became solid with higher concentrations, not absorbing all buffer.

(a) 33% BC. **(b)** 49% BC. **(c)** 57% BC.

Figure 4.16: Images of three 5:95 ASDs with varying acidic buffer concentration (BC) after 24 h. The 33% sample is translucent. Higher buffer concentration increases turbidity, eventually resulting in a "milky" sample.

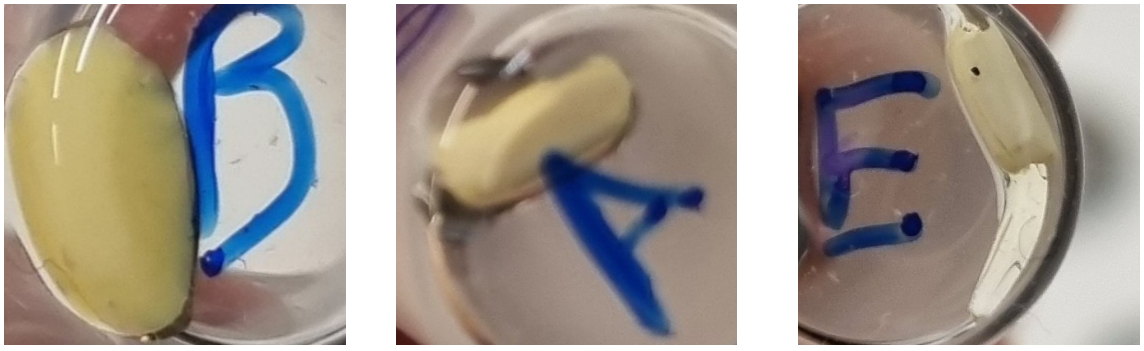

(a) 30% BC. **(b)** 47% BC. **(c)** 64% BC.

Figure 4.17: Images of three 30:70 ASDs with varying acidic buffer concentration (BC) after 24 h. All samples are opaque. For higher buffer concentration, the ASDs did not absorb all buffer after 24 hours.

SAXS and WAXS was performed on the hydrated samples, to observe any nanoscale phase separation. Fig. 4.18 shows characteristic SAXS and WAXS curves of each ASD. All measurements can be seen in Fig. A.12–A.15. Generally, the SAXS measurements have either a constant decline or low signal, indicating no nanoscale heterogeneities. The measurements vary in slope at low q, which can be attributed to different surface scattering contributions from objects larger than the detectable range of SAXS. The WAXS curves show broad peaks, indicating that the samples are amorphous. Consequently, no measurement showed any indication of nanoscale phase separation or crystallisation.

Clearly, larger scale phase separation occurs in these samples that could not be seen in SAXS. The pH dependence of the phase separation likely originates from the pH dependence of the solubility of indomethacin. As the solubility in acidic media is lower in comparison to neutral media, there is a larger miscibility gap between drug and dissolution media. One can hypothesise that this leads to larger and more distinct drug-rich regions. In the previous section it was showed that the

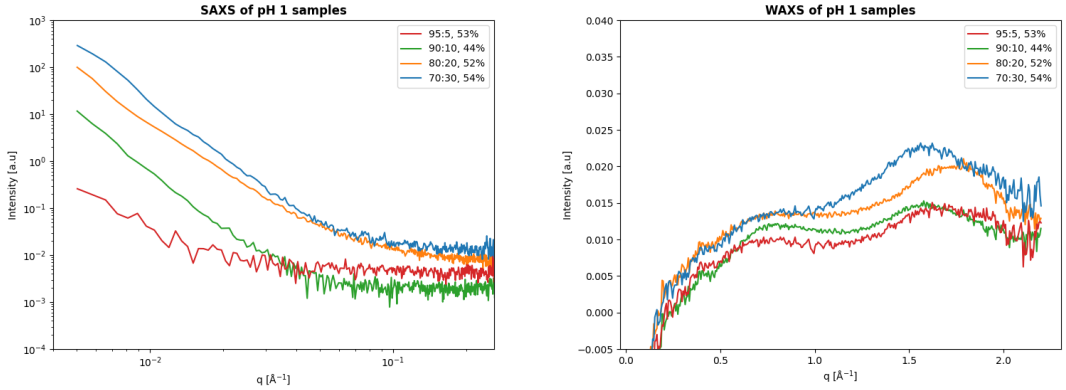

(a) SAXS **(b)** WAXS

Figure 4.18: Characteristic X-ray scattering measurements of hydrated ASDs with varying concentration of acidic dissolution media.

drug load and consequently phase separation affected the dissolution behaviour in neutral media to some degree. There, the drug-rich regions have a characteristic length scale up to $\sim 50\,\text{nm}$. In pH 1, the characteristic length scale is larger. Tres et al. and Saboo et al. attributed the poor dissolution behaviour of IND:PVPVA ASDs in acidic dissolution media to phase separation, leading to a drug-rich hydrophobic surface upon dissolution [5], [7]. Consequently, it seems that in order for phase separation to have a large effect on dissolution behaviour, it needs to be on a larger scale.

4.3 Humidity stressed samples

SAXS and WAXS was used to analyse phase separation in ASDs exposed to humid envionments, as it has been reported to be detrimental to long-term stability. Fig. 4.19 shows the SAXS measurements of these. The samples exposed to 75% RH had absorbed up to 17% water. All samples remained translucent. The 5:95 was transparent and gel-like with a faint yellow tint, while the 30:70 sample was solid, Fig. A.16. The samples exposed to 98% RH were gel-like, having absorbed up to 24% water. This level of absorption is similar to the ASDs with T_g close to room temperature, indicating that these are on the verge of becoming super-cooled liquids. The 5:95 sample became fully transparent, while the 30:70 sample hade a distinct yellow tint. There were no signs of crystallisation, based on the WAXS curves in Fig. 4.20. No samples had become opaque, indicating that there was no phase separation on the visible scale. No features indicating a characteristic lengthscale were observed in the SAXS curves of the 75% RH samples, seen in Fig. 4.19a. The SAXS curves of the 98% RH case can be seen in Fig. 4.19b. The 5:95 measurement only consist of noise, indicating that the samples is dissolved. The 30:70 measurement exhibits a broad shoulder, indicating polydisperse heterogeneities. The absorbed water concentration is lower than the lowest buffer concentration for the 30:70 samples, indicating that heterogeneities are induced earlier than shown in the phase diagram.

Generally, after exposure to high humidity, the IND:PVPVA remain amorphous, and only the samples with high drug load in high humidity may exhibit nanoscale phase separation. This phase separation is not inherently detrimental to dissolution, as shown in the previous section. It has previously been shown to lead to crystallisation over time. However, here it is shown that exposure to a humid environment does not lead to crystallisation of ASDs after 10 weeks.

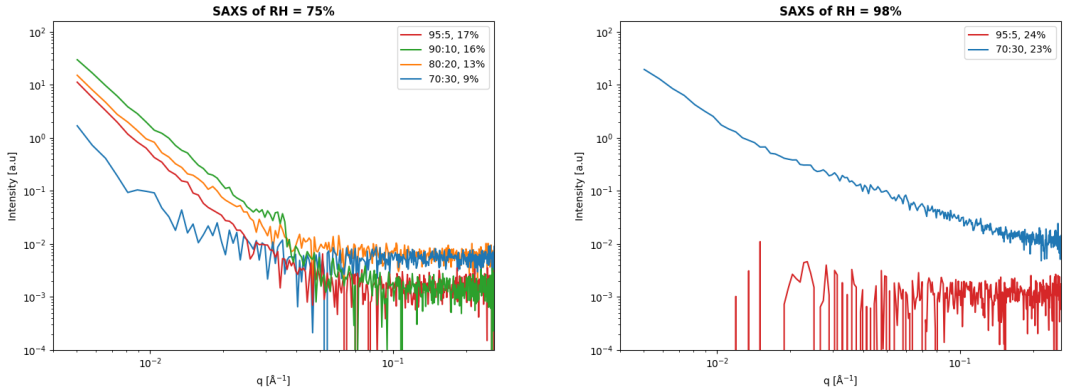

(a) 75% relative humidity **(b)** 98% relative humidity

Figure 4.19: SAXS measurements of humidity stressed ASDs.

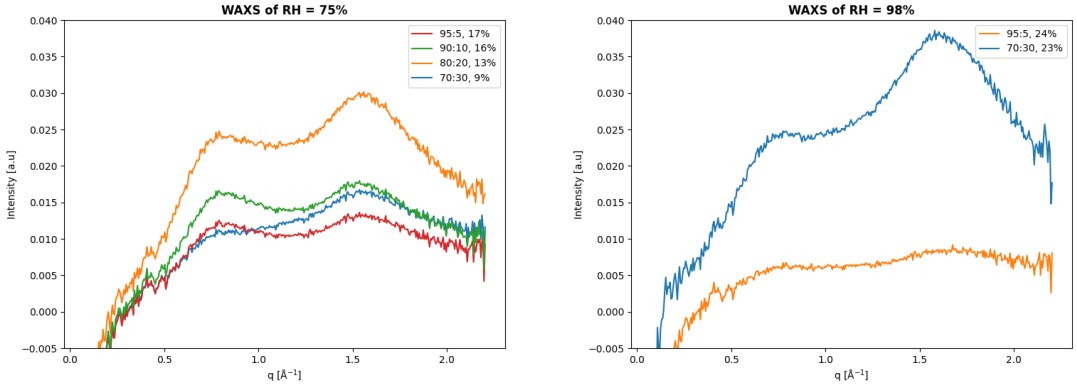

(a) 75% relative humidity **(b)** 98% relative humidity

Figure 4.20: WAXS measurements of humidity stressed ASDs.

5

Conclusion

Phase separation in amorphous solid dispersions has been shown to affect dissolution properties and long-term stability. It has previously been reported to be detrimental to drug release in acidic dissolution media. As the drug-poor domains dissolve, a drug-rich shell is created, inhibiting drug release. This thesis can conclude that phase separation in IND:PVPVA ASDs is also induced by neutral dissolution media, for high enough drug loads. For low drug loads, up to 5w% indomethacin, no phase separation is seen and the sample eventually dissolves in the dissolution media. ASDs with drug load between 10 and 30w% start to phase separate as dissolution media is absorbed. In SAXS curves, this is indicated by the presence of broad shoulders. This phase separation can be characterised with an approximate lengthscale which corresponds to the centre of the bump. This ranges between 8 and 50 nm, and does not correlate with buffer concentration. However, the average lengthscale seem to correlate with drug load. For 10w%, i.e. the 10:90 samples, this phase separation is seen between 40% and 65% buffer concentration. A higher buffer concentration seem to dissolve the sample. This phase separation is seen in the 20:80 samples up to 55% buffer concentration, and up to 50% for the 30:70 samples. Generally, the morphology of the phase separation can be described as having a distribution of lengthscales on the nanoscale, without distinct interfaces.

With higher buffer concentration for the 20:80 and 30:70 ASDs, the phase separation is clearer. It can here be characterised with a distinct lengthscale, which can be seen in the SAXS curves as a shoulder. This lengthscale does not vary significantly with varying buffer concentration, while it increases with drug load. For 20:80, it is ~ 35 nm, and ~ 50 nm for 30:70. The slope is -4 in the Porod region, indicating a clear interface between the domains. It is hypothesised that when a certain buffer concentration is reached, the drug-rich domains are stable. The additional absorbed buffer enters the drug-poor regions, while the drug-rich region is stable.

In comparison to the acidic dissolution media, the phase separation described above does not inhibit drug release. The distinct phase separation might affect the early drug release for 20:80 and 30:70. However, all ASDs have good dissolution behaviour as they dissolve within 10 minutes. Consequently, the phase separation induced by neutral dissolution media is not detrimental to drug release. The phase separation differs from the one induced by acidic media. SAXS measurements of ASDs with acidic buffer did not show any distinct features, suggesting that the lengthscales are

outside the detectable q-range. The samples became opaque after a certain amount of added buffer, indicating a larger scale heterogeneity. These observations support that phase separation in ASDs under acidic conditions generally occurs at larger lengthscales. Further studying of the phase separation induced by acidic dissolution media with instruments that offer micrometer resolution could give more insight into the mechanisms and morphology.

Finally, the stability of the ASDs was tested as they were exposed to a humid environment. Most of the sample did not show any heterogeneity. Only 30:70 showed phase separation when it was exposed to 98% relative humidity for 10 weeks. This phases separation is polydisperse, similar to the first one described above. This showcased the stability of ASDs. The induced phase separation does not likely inhibit drug release, and is shown here not to lead to crystallisation after 10 weeks.

Bibliography

[1] H. D. Williams, N. L. Trevaskis, S. A. Charman, *et al.*, "Strategies to address low drug solubility in discovery and development," *Pharmacological Reviews*, vol. 65, no. 1, pp. 315–499, 2013, ISSN: 0031-6997. DOI: https://doi.org/10.1124/pr.112.005660.

[2] G. Van den Mooter, "The use of amorphous solid dispersions: A formulation strategy to overcome poor solubility and dissolution rate," *Drug Discovery Today: Technologies*, vol. 9, no. 2, e79–e85, 2012, Formulation technologies to overcome poor drug-like properties, ISSN: 1740-6749. DOI: https://doi.org/10.1016/j.ddtec.2011.10.002.

[3] S. Baghel, H. Cathcart, and N. J. O'Reilly, "Polymeric amorphous solid dispersions: A review of amorphization, crystallization, stabilization, solid-state characterization, and aqueous solubilization of biopharmaceutical classification system class ii drugs," *Journal of Pharmaceutical Sciences*, vol. 105, no. 9, pp. 2527–2544, 2016, ISSN: 0022-3549. DOI: https://doi.org/10.1016/j.xphs.2015.10.008.

[4] Q. Fu, H.-D. Lu, Y.-F. Xie, *et al.*, "Salt formation of two bcs ii drugs (indomethacin and naproxen) with (1r, 2r)-1,2-diphenylethylenediamine: Crystal structures, solubility and thermodynamics analysis," *Journal of Molecular Structure*, vol. 1185, pp. 281–289, 2019, ISSN: 0022-2860. DOI: https://doi.org/10.1016/j.molstruc.2019.02.104.

[5] F. Tres, K. Treacher, J. Booth, *et al.*, "Indomethacin-kollidon va64 extrudates: A mechanistic study of ph-dependent controlled release," *Molecular Pharmaceutics*, vol. 13, no. 3, pp. 1166–1175, 2016, PMID: 26845251. DOI: 10.1021/acs.molpharmaceut.5b00979. eprint: https://doi.org/10.1021/acs.molpharmaceut.5b00979.

[6] National Center for Biotechnology Information, *Pubchem compound summary for cid 270885, pvp-va*, https://pubchem.ncbi.nlm.nih.gov/compound/Pvp-VA, Accessed: 2025-05-12, 2025.

[7] S. Saboo, U. S. Kestur, D. P. Flaherty, and L. S. Taylor, "Congruent Release of Drug and Polymer from Amorphous Solid Dispersions: Insights into the Role of Drug-Polymer Hydrogen Bonding, Surface Crystallization, and Glass Transition," *Molecular Pharmaceutics*, vol. 17, no. 4, pp. 1261–1275, Apr. 2020,

Publisher: American Chemical Society, ISSN: 1543-8384. DOI: 10.1021/acs.molpharmaceut.9b01272.

[8] A. C. F. Rumondor, H. Wikström, B. Van Eerdenbrugh, and L. S. Taylor, "Understanding the Tendency of Amorphous Solid Dispersions to Undergo Amorphous–Amorphous Phase Separation in the Presence of Absorbed Moisture," en, *AAPS PharmSciTech*, vol. 12, no. 4, pp. 1209–1219, Dec. 2011, ISSN: 1530-9932. DOI: 10.1208/s12249-011-9686-y. (visited on 05/26/2025).

[9] N. Shah, H. Sandhu, D. S. Choi, H. Chokshi, and A. W. Malick, Eds., *Amorphous Solid Dispersions: Theory and Practice* (Advances in Delivery Science and Technology). New York, NY: Springer, 2014, ISBN: 978-1-4939-1597-2. DOI: 10.1007/978-1-4939-1598-9.

[10] H. Patil, R. V. Tiwari, and M. A. Repka, "Hot-Melt Extrusion: From Theory to Application in Pharmaceutical Formulation," en, *AAPS PharmSciTech*, vol. 17, no. 1, pp. 20–42, Feb. 2016, ISSN: 1530-9932. DOI: 10.1208/s12249-015-0360-7. (visited on 04/23/2025).

[11] M. D. Ediger, C. A. Angell, and S. R. Nagel, "Supercooled liquids and glasses," *The Journal of Physical Chemistry*, pp. 13 200–13 212, Jan. 1996. DOI: https://doi.org/10.1021/jp953538d.

[12] L. Yu, "Amorphous pharmaceutical solids: Preparation, characterization and stabilization," *Advanced Drug Delivery Reviews*, vol. 48, no. 1, pp. 27–42, 2001, Characterization of the Solid State, ISSN: 0169-409X. DOI: https://doi.org/10.1016/S0169-409X(01)00098-9.

[13] L. S. Taylor and G. G. Zhang, "Physical chemistry of supersaturated solutions and implications for oral absorption," en, *Advanced Drug Delivery Reviews*, vol. 101, pp. 122–142, Jun. 2016, ISSN: 0169409X. DOI: 10.1016/j.addr.2016.03.006. (visited on 03/10/2025).

[14] C. Sagui, D. O'Gorman, and M. Grant, "Nucleation, growth, and coarsening in phase separating systems," *Scanning Microsc.*, vol. 12, pp. 3–8, Jan. 1998.

[15] J. W. Cahn, "On spinodal decomposition," *Acta Metallurgica*, vol. 9, no. 9, pp. 795–801, 1961, ISSN: 0001-6160. DOI: https://doi.org/10.1016/0001-6160(61)90182-1.

[16] H. S. Purohit and L. S. Taylor, "Phase Separation Kinetics in Amorphous Solid Dispersions Upon Exposure to Water," *Molecular Pharmaceutics*, vol. 12, no. 5, pp. 1623–1635, May 2015, Publisher: American Chemical Society, ISSN: 1543-8384. DOI: 10.1021/acs.molpharmaceut.5b00041. (visited on 04/10/2025).

[17] A. Schittny, J. Huwyler, and M. Puchkov, "Mechanisms of increased bioavailability through amorphous solid dispersions: A review," *Drug Delivery*, vol. 27, no. 1, pp. 110–127, Jan. 2020, Publisher: Taylor & Francis _eprint: https://doi.org/10.1080/107
ISSN: 1071-7544. DOI: 10.1080/10717544.2019.1704940. (visited on 01/24/2025).

[18] National Center for Biotechnology Information, *Pubchem compound summary for cid 3715, indomethacin*, https://pubchem.ncbi.nlm.nih.gov/compound/Indomethacin, Accessed: 2025-04-28, 2024.

[19] S. K. Singh, A. K. Singh, and S. K. Singh, "Emerging role of biopharmaceutical classification and biopharmaceutics drug disposition classification system in drug development," *Journal of Advanced Pharmaceutical Technology and Research*, vol. 13, no. 4, pp. 252–258, 2022. DOI: 10.4103/japtr.japtr_105_22.

[20] D. D. Sun and P. I. Lee, "Probing the mechanisms of drug release from amorphous solid dispersions in medium-soluble and medium-insoluble carriers," *Journal of Controlled Release*, vol. 211, pp. 85–93, 2015, ISSN: 0168-3659. DOI: https://doi.org/10.1016/j.jconrel.2015.06.004.

[21] E. Fritschka and G. Sadowski, "Rigorous modeling the ph-dependent solubility of weak acids, weak bases and their salts," *Fluid Phase Equilibria*, vol. 580, p. 114 039, 2024, ISSN: 0378-3812. DOI: https://doi.org/10.1016/j.fluid.2024.114039.

[22] X. Yuan, T.-X. Xiang, B. D. Anderson, and E. J. Munson, "Hydrogen Bonding Interactions in Amorphous Indomethacin and Its Amorphous Solid Dispersions with Poly(vinylpyrrolidone) and Poly(vinylpyrrolidone-co-vinyl acetate) Studied Using 13C Solid-State NMR," *Molecular Pharmaceutics*, vol. 12, no. 12, pp. 4518–4528, Dec. 2015, Publisher: American Chemical Society, ISSN: 1543-8384. DOI: 10.1021/acs.molpharmaceut.5b00705. (visited on 05/12/2025).

[23] National Center for Biotechnology Information, *Pubchem substance record for sid 135274158, copovidone [ban:nf], source: Chemidplus*, https://pubchem.ncbi.nlm.nih.gov/substance/135274158, Accessed June 13, 2025, 2025.

[24] T. Matsumoto and G. Zografi, "Physical Properties of Solid Molecular Dispersions of Indomethacin with Poly(vinylpyrrolidone) and Poly(vinylpyrrolidone-co-vinyl-acetate) in Relation to Indomethacin Crystallization," en, *Pharmaceutical Research*, vol. 16, no. 11, pp. 1722–1728, Nov. 1999, ISSN: 1573-904X. DOI: 10.1023/A:1018906132279. (visited on 05/12/2025).

[25] R. Pezzoli, J. G. Lyons, N. Gately, and C. L. Higginbotham, "Investigation of miscibility estimation methods between indomethacin and poly(vinylpyrrolidone-co-vinyl acetate)," *International Journal of Pharmaceutics*, vol. 549, no. 1, pp. 50–57, 2018, ISSN: 0378-5173. DOI: https://doi.org/10.1016/j.ijpharm.2018.07.039.

[26] G. W. H. Höhne, W. F. Hemminger, and H.-J. Flammersheim, *Differential Scanning Calorimetry*. Springer Berlin, Heidelberg, 2013, ISBN: 978-3-662-06710-9. DOI: https://doi.org/10.1007/978-3-662-06710-9.

[27] A. Paar, *The SAXS Guide: Getting Acquainted with the Principles*. Anton Paar GmbH, 2013. [Online]. Available: https://www.anton-paar.com/us-en/saxs-guide/.

[28] U.S. Food and Drug Administration, *Dissolution testing of immediate release solid oral dosage forms*, Guidance for Industry, 1997. [Online]. Available: https://www.fda.gov/regulatory-information/search-fda-guidance-documents/dissolution-testing-immediate-release-solid-oral-dosage-forms.

[29] S. Patel, A. Raulji, D. Patel, D. Panchal, M. Dalwadi, and U. Upadhyay, "A review on "uv visible spectroscopy," *International Journal of Pharmaceutical Research and Applications*, vol. 7, no. 5, pp. 1144–1151, 2022, ISSN: 2456-4494. DOI: 10.35629/7781-070511441151.

[30] F. Qian, J. Huang, and M. A. Hussain, "Drug–polymer solubility and miscibility: Stability consideration and practical challenges in amorphous solid dispersion development," *Journal of Pharmaceutical Sciences*, vol. 99, no. 7, pp. 2941–2947, 2010, ISSN: 0022-3549. DOI: https://doi.org/10.1002/jps.22074.

A

Appendix

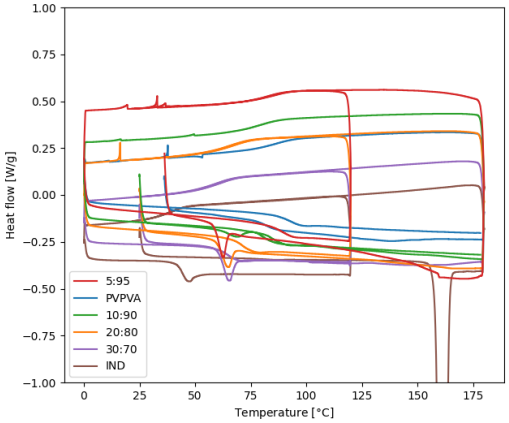

Figure A.1: Full DSC of the pristine samples.

Table A.1: All hydrated samples with neutral buffer.

SAMPLE	BUFFER CONCENTRATION (%)														
PVPVA	37	45	55	58	64										
5:95	33	39	48	50	50	51	53	58	61						
10:90	28	37	41	42	48	50	51	53	54	55	59	60	61	65	68
20:80	27	37	41	48	50	50	52	53	54	58	60	62	66	71	71
30:70	28	37	37	44	45	46	47	50	51	53	55	58	61	64	72

Table A.2: All hydrated samples with acidic buffer.

SAMPLE	BUFFER CONCENTRATION (%)							
5:95	33	41	48	53	62	66		
10:90	28	37	44	47	51	57	62	69
20:80	28	35	45	50	52	56	60	65
30:70	20	28	39	47	54	63		

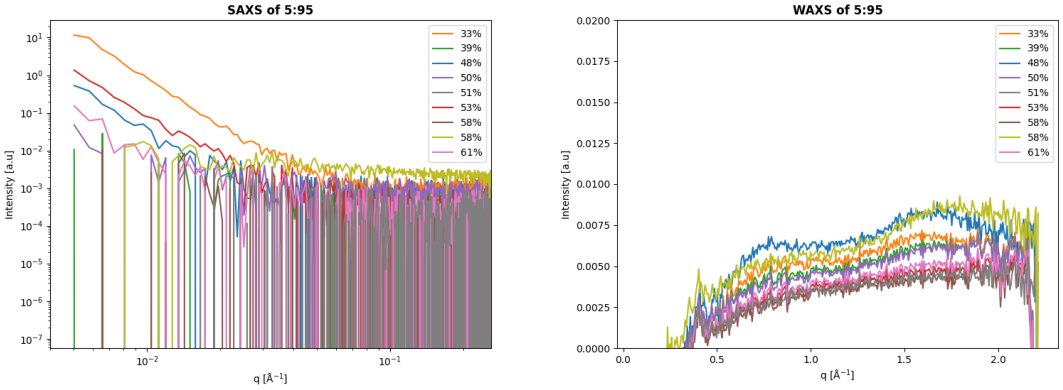

(a) SAXS **(b)** WAXS

Figure A.2: X-ray scattering measurements of all wet samples of 5:95 ASDs.

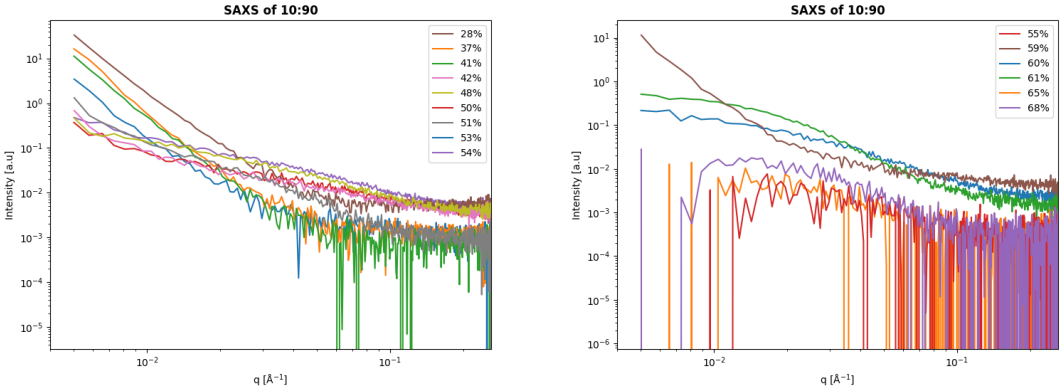

(a) <50% **(b)** >50%

Figure A.3: SAXS measurements of all wet samples of 10:90 ASDs.

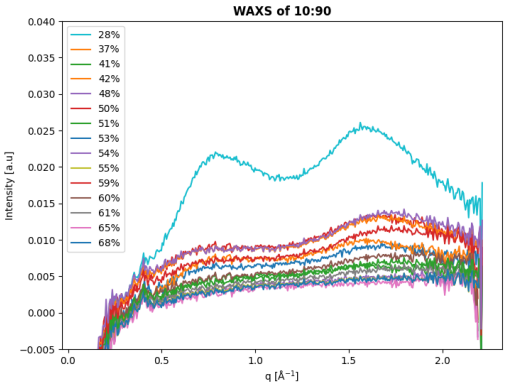

Figure A.4: WAXS measurements of all wet samples of 10:90 ASDs.

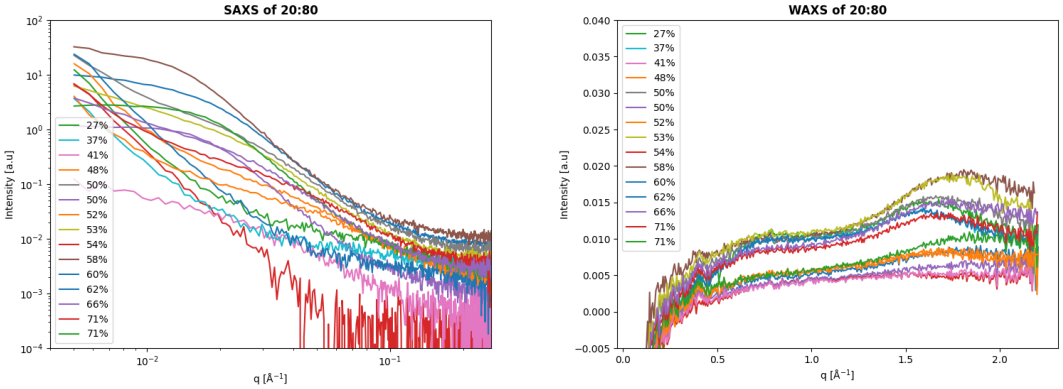

(a) SAXS **(b)** WAXS

Figure A.5: X-ray scattering measurements of all wet samples of 20:80 ASDs.

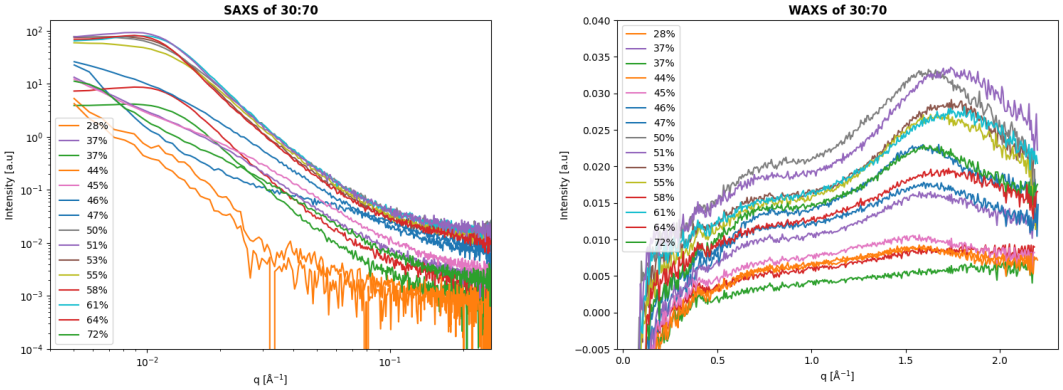

(a) SAXS **(b)** WAXS

Figure A.6: X-ray scattering measurements of all wet samples of 30:70 ASDs.

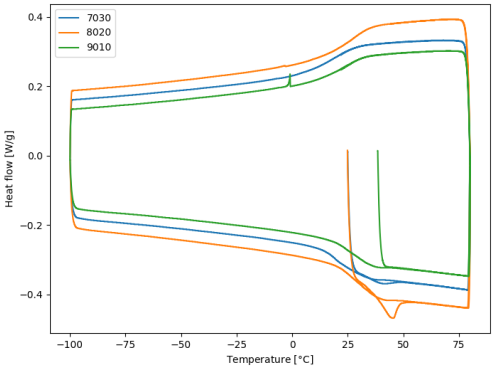

Figure A.7: Full DSC of the wet samples.

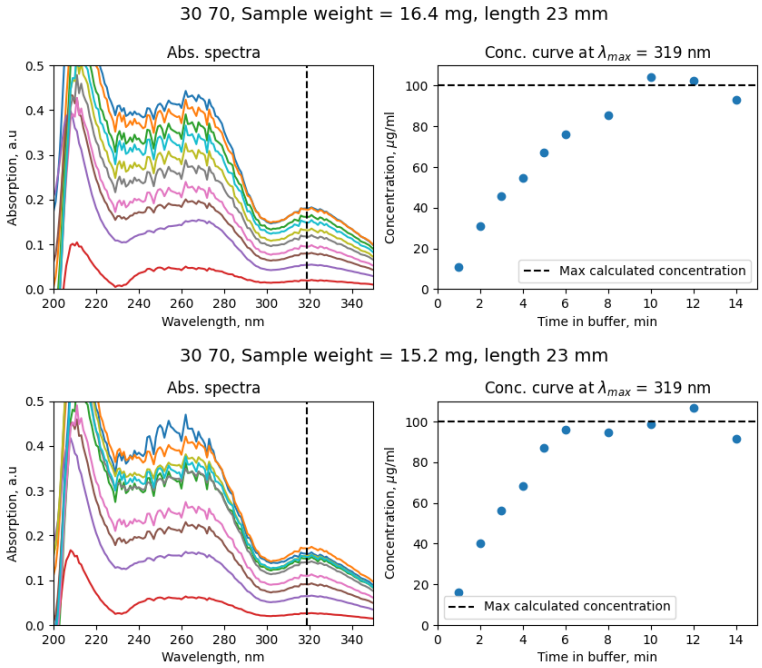

Figure A.8: Absorption and concentration curves for the two 30:70 samples.

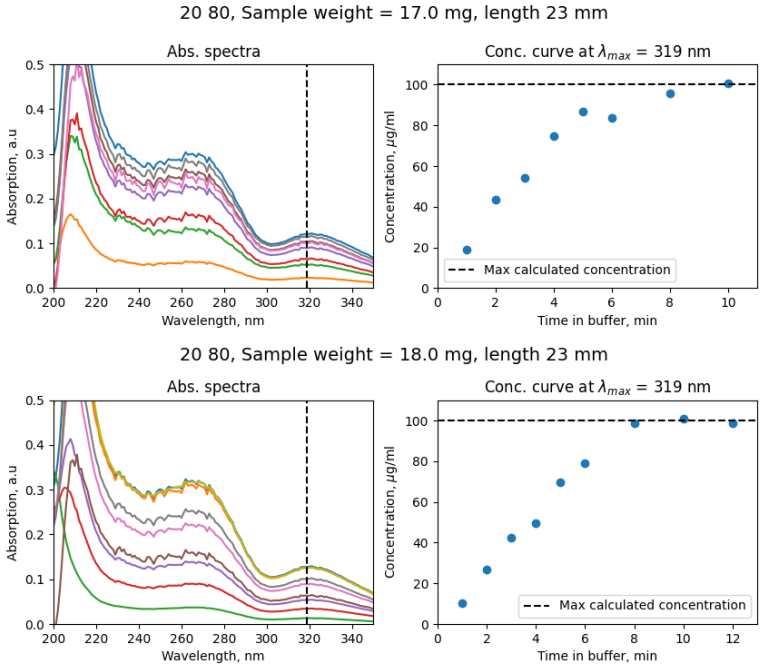

Figure A.9: Absorption and concentration curves for the two 20:80 samples.

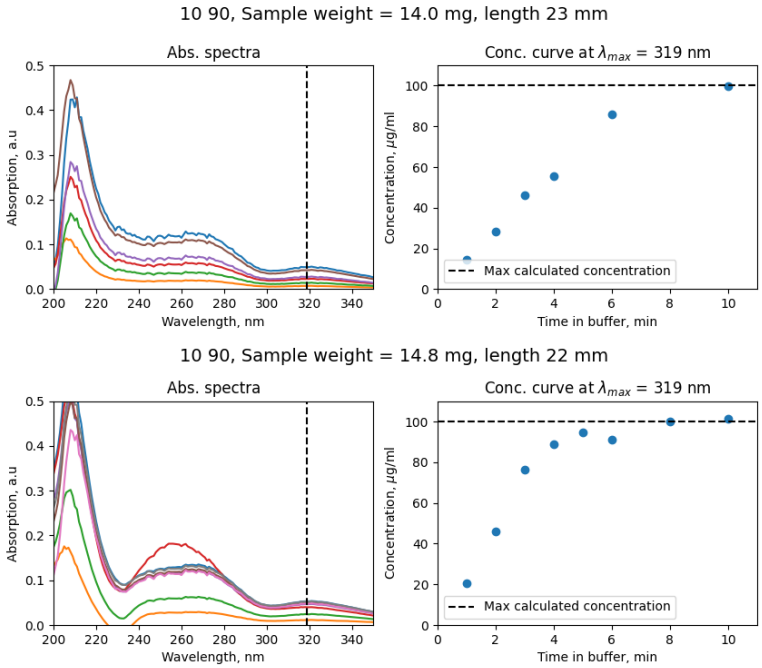

Figure A.10: Absorption and concentration curves for the two 10:90 samples.

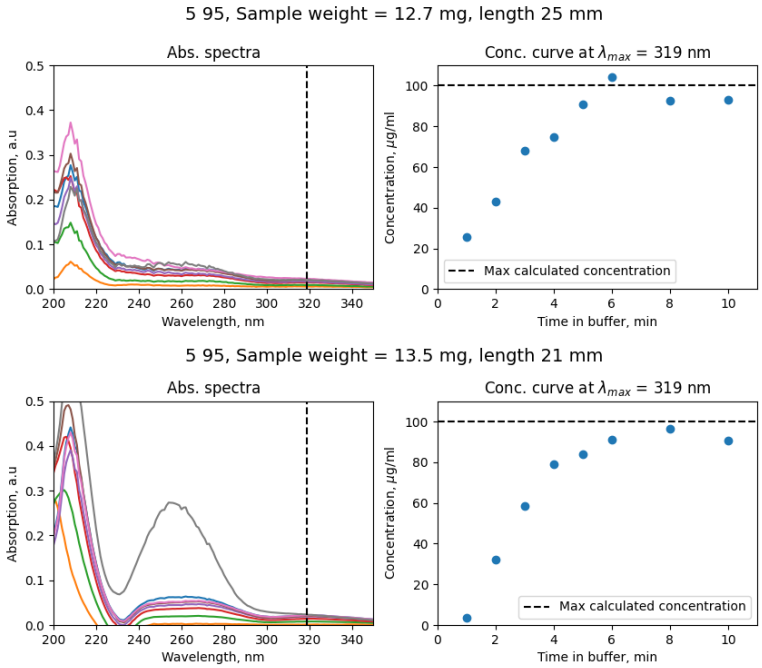

Figure A.11: Absorption and concentration curves for the two 5:95 samples.

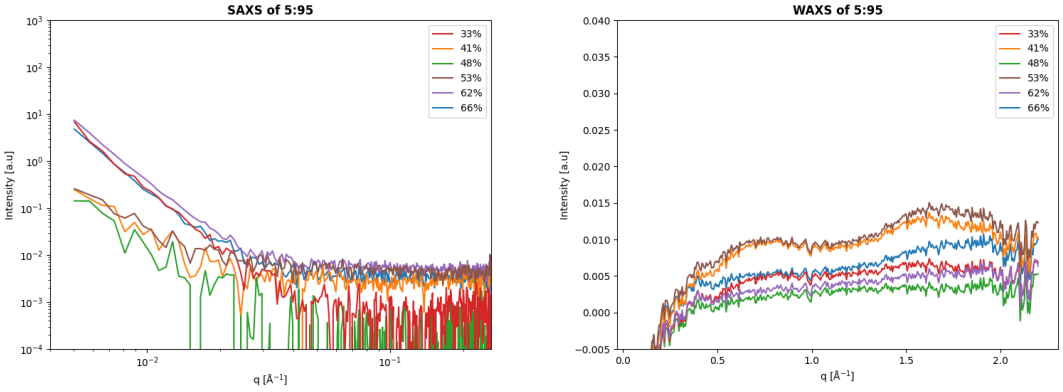

(a) SAXS **(b)** WAXS

Figure A.12: X-ray scattering measurements of 5:95 ASDs in acidic dissolution media.

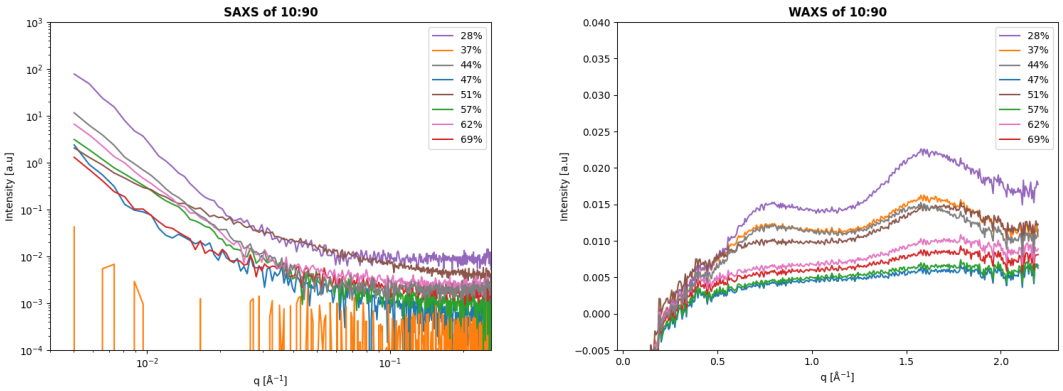

(a) SAXS **(b)** WAXS

Figure A.13: X-ray scattering measurements of 10:90 ASDs in acidic dissolution media.

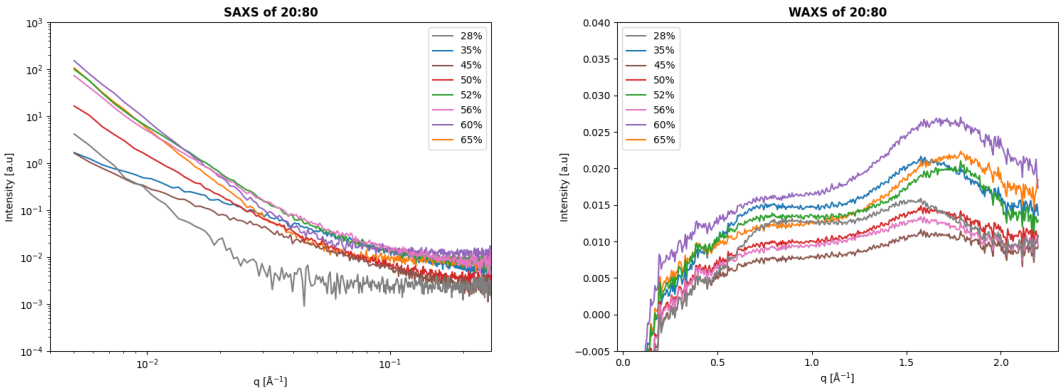

(a) SAXS **(b)** WAXS

Figure A.14: X-ray scattering measurements of 20:80 ASDs in acidic dissolution media.

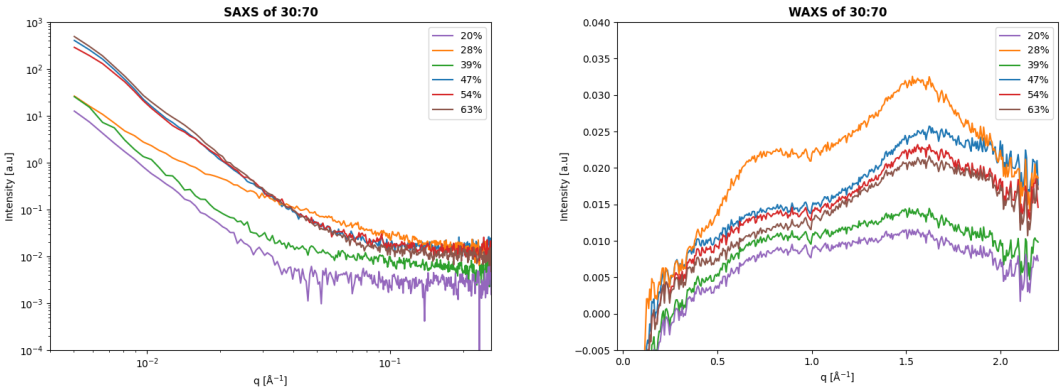

(a) SAXS **(b)** WAXS

Figure A.15: X-ray scattering measurements of 30:70 ASDs in acidic dissolution media.

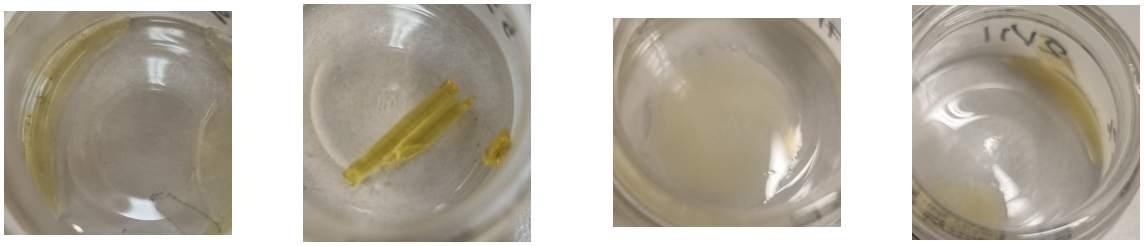

(a) 5:95 ASD in RH=75%.

(b) 30:70 ASD in RH=75%.

(c) 5:95 ASD in RH=98%.

(d) 30:70 ASD in RH=98%.

Figure A.16: Images of the humidity stressed samples.

DEPARTMENT OF PHYSICS
CHALMERS UNIVERSITY OF TECHNOLOGY
Gothenburg, Sweden
www.chalmers.se

CHALMERS
UNIVERSITY OF TECHNOLOGY